Journal of Theoretical Biology 266 (2010) 641–656

Contents lists available at ScienceDirect

Journal of Theoretical Biology

journal homepage: www.elsevier.com/locate/yjtbi

Attractor analysis of asynchronous Boolean models of signal transduction networks

Assieh Saadatpour [a], István Albert [b], Réka Albert [b,c,*]

[a] Department of Mathematics, The Pennsylvania State University, University Park, PA 16802, USA
[b] Department of Physics and Huck Institutes of the Life Sciences, The Pennsylvania State University, University Park, PA 16802, USA
[c] Department of Physics, The Pennsylvania State University, University Park, PA 16802, USA

ARTICLE INFO

Article history:
Received 17 October 2009
Received in revised form
28 May 2010
Accepted 21 July 2010
Available online 24 July 2010

Keywords:
Boolean network model
Dynamic analysis
Synchronous model
Asynchronous model
Abscisic acid signal transduction network

ABSTRACT

Prior work on the dynamics of Boolean networks, including analysis of the state space attractors and the basin of attraction of each attractor, has mainly focused on synchronous update of the nodes' states. Although the simplicity of synchronous updating makes it very attractive, it fails to take into account the variety of time scales associated with different types of biological processes. Several different asynchronous update methods have been proposed to overcome this limitation, but there have not been any systematic comparisons of the dynamic behaviors displayed by the same system under different update methods. Here we fill this gap by combining theoretical analysis such as solution of scalar equations and Markov chain techniques, as well as numerical simulations to carry out a thorough comparative study on the dynamic behavior of a previously proposed Boolean model of a signal transduction network in plants. Prior evidence suggests that this network admits oscillations, but it is not known whether these oscillations are sustained. We perform an attractor analysis of this system using synchronous and three different asynchronous updating schemes both in the case of the unperturbed (wild-type) and perturbed (node-disrupted) systems. This analysis reveals that while the wild-type system possesses an update-independent fixed point, any oscillations eventually disappear unless strict constraints regarding the timing of certain processes and the initial state of the system are satisfied. Interestingly, in the case of disruption of a particular node all models lead to an extended attractor. Overall, our work provides a roadmap on how Boolean network modeling can be used as a predictive tool to uncover the dynamic patterns of a biological system under various internal and environmental perturbations.

© 2010 Elsevier Ltd. All rights reserved.

1. Introduction

Network modeling has demonstrated its utility for analyzing molecular and cellular level biological systems by integrating the existing knowledge into a single representation (Giot et al., 2003; Lee et al., 2002; Li et al., 2004). In this network representation, the components of a system of interest (e.g. proteins, mRNAs, and molecules) serve as the nodes while the interactions among the nodes are described by edges. This type of abstraction can provide a foundation for developing computational approaches that are able to predict the dynamic behavior of a biological system in response to environmental stimuli and internal perturbations. Continuous and deterministic approaches, usually formulated as a system of ordinary differential equations, are well suited for small and well-characterized systems with known kinetic parameters (Chen et al., 2000; von Dassow et al., 2000). Alternatively, discrete dynamic modeling has been increasingly employed when analyzing biological systems with many unknown components and parameters such as large-scale gene regulatory and signal transduction networks (Mendoza and Alvarez-Buylla, 2000; Song et al., 2009; Willadsen and Wiles, 2007; Zhang et al., 2008). The most widely used discrete dynamic framework assumes only two qualitative states for each node, denoted by ON (1) and OFF (0). These so-called Boolean networks were pioneered by Kauffman (1969) and Thomas (1973) as models of gene regulatory networks.

The simplest form of a Boolean model, known as a synchronous model (Kauffman, 1993), assumes similar time scales for all the processes involved, and is implemented by updating all the nodes' states simultaneously. However, this assumption is often unrealistic in many molecular interaction systems where a variety of time scales, from fractions of a second to hours, are needed to correctly represent the phenomena of interest. For example, signaling activities such as kinase/phosphatase reactions, protein conformational changes and the physical movement of signaling

* Corresponding author at: The Pennsylvania State University, Department of Physics and Huck Institutes of the Life Sciences, University Park, PA 16802, USA. Tel.: +1 8148656123; fax: +1 8148653604.
E-mail address: ralbert@phys.psu.edu (R. Albert).

0022-5193/$ - see front matter © 2010 Elsevier Ltd. All rights reserved.
doi:10.1016/j.jtbi.2010.07.022

compounds occur over a time frame ranging from fractions of a second to seconds. Signaling responses that are coupled with metabolic processes can arise in fractions of a second, while transcriptional events, receptor internalization, and cellular growth require hundreds of seconds or longer to occur (Papin et al., 2005).

The need to represent various time scales motivated the development of asynchronous models (Thomas, 1973) that add more variability to the update order. Prominent examples include stochastic updates such as the random order asynchronous (Chaves et al., 2005; Harvey and Bossomaier, 1997; Li et al., 2006; Thakar et al., 2007; Zhang et al., 2008) and general asynchronous (Harvey and Bossomaier, 1997) update methods. Several deterministic asynchronous methods were also studied, in which the nodes are updated in a pre-determined sequence (Aracena et al., 2009; Mortveit and Reidys, 2007) or at multiples of their corresponding pre-selected time units (Chaves et al., 2006). In addition, to avoid the complexity associated with some asynchronous models a recent study has incorporated activation and degradation time delays through introducing "dummy" nodes into the synchronous Boolean network model of the budding yeast cell cycle (Irons, 2009). Two other classes of time- and space-discrete dynamical systems for which synchronous and asynchronous updating schemes have been employed are sequential dynamical systems (Mortveit and Reidys, 2007) and cellular automata (Matache and Heidel, 2005; Schonfisch and de Roos, 1999). The underlying graph for the former is undirected, and the latter is typically defined on regular lattices or grids, and in both cases the transfer functions are usually the same for all the nodes.

The dynamical properties of synchronous Boolean networks, including analysis of the attractors in the state space of the system and their corresponding basin of attraction, have been well studied (Dubrova and Teslenko, 2010; Faure et al., 2006; Garg et al., 2008; Heidel et al., 2003; Klemm and Bornholdt, 2005; Wuensche, 2002). However, the majority of the current studies on asynchronous Boolean models have mainly focused on finding the fixed points of the system or on identifying the fixed points reachable from the nominal (wild-type) initial condition (Chaves et al., 2005). Very few studies set their goals to identify cycles (Faure et al., 2006; Garg et al., 2008) and no study that we are aware of provides a thorough exploration of the basin of attraction of cycles. Thus, the investigation of all possible attractors and their basins of attraction for a system under different updating schemes is still an open question. Here we have performed a comprehensive study of all attractors of a biological system, considering every possible initial state, using a synchronous and three asynchronous Boolean models.

The biological system that we chose for this analysis is the signal transduction network corresponding to drought response in plants. Plants take up carbon dioxide and can lose water through microscopic pores called stomata. The surrounding pair of so-called guard cells plays a crucial role in controlling the stomatal size. During drought, the plant hormone abscisic acid (ABA) is synthesized to promote stomatal closure, thus cutting down evaporation from the interior of the plant (Li et al., 2006). In addition to the importance of stomata in control of the plant water balance, study of the stomatal opening and closing in response to various stimuli like ABA is of particular interest to biologists as it can be readily used to test different hypotheses for mechanisms affecting signal transduction (Schroeder et al., 2001). A comprehensive reconstruction of the signaling network responsible for ABA-induced stomatal closure was previously performed by Li et al. (2006). The 54 nodes of the network are comprised of proteins, ion channels and secondary messengers, and a few conceptual nodes such as plasma membrane depolarization and stomatal closure. The edges of this network, the vast majority of them directed, represent protein–protein interactions, chemical reactions, and indirect regulatory relationships between two nodes. Li et al. (2006) also developed a Boolean model for the ABA signaling network and performed random order asynchronous simulations, focusing on the behavior of a single node, representing stomatal closure.

One of the interesting features of the ABA signal transduction network is the possible existence of Ca^{2+}-driven oscillations in a subset of the nodes. Among the many signaling mechanisms associated with Ca^{2+} (Berridge et al., 2000), calcium oscillations and waves have been frequently observed in muscle cells and neurons (Morita et al., 1980), mammalian embryonic development (Cuthbertson and Cobbold, 1985; Jones, 1998) as well as plant cells (McAinsh et al., 1995). While cytosolic Ca^{2+} (denoted by Ca_c^{2+}) fluctuations have been observed in stomatal guard cells, there are indications that Ca_c^{2+} oscillation may be more important for the maintenance of closure than for the induction of closure (Allen et al., 2001) and that the induction of closure might only depend on the first, transient Ca_c^{2+} elevation. The model of Li et al. (2006) predicted that when Ca_c^{2+} elevation occurs, stomatal closure is triggered; however, neither Ca_c^{2+} oscillation nor Ca_c^{2+} elevation is required for ABA-induced stomatal closure in the model. Nevertheless, Li et al. (2006) do conclude that Ca_c^{2+} modulation confers an essential redundancy to the network, as Ca_c^{2+} elevation becomes required for engendering stomatal closure when pH_c changes, K^+ efflux or the S1P-PA pathway are perturbed.

In this work, we have performed a systematic study of the long-term dynamic behavior supported by the ABA-induced closure model developed by Li et al. (2006), with a special focus on the possibility of long-term oscillations. To this end, we employed synchronous as well as three different asynchronous updating techniques, i.e., random order asynchronous (ROA), general asynchronous (GA), and deterministic asynchronous (DA) methods. In the ROA method, at each round of update a random ordered sequence of the nodes is selected and the nodes are updated in that order. In the GA method, at each time step a randomly selected node is updated, and in the DA method nodes are updated only at multiples of their corresponding pre-selected time units. Our analysis reveals a significant degree of dependence of the model's behavior on the manner of update as an overlapping but non-identical set of attractors emerged for the various updating schemes. This diversity in dynamical behavior is also observed when exploring the impact of deleting (knocking out) biologically significant nodes. For instance, disrupting certain nodes will lead to a fixed point or sustained oscillations (depending on the initial condition) in the synchronous model, while the same disruption modeled with the ROA or GA methods will produce the same fixed point but no oscillations. This study provides a comprehensive comparison and novel insights into the dynamical features of various Boolean models through capturing the diverse behaviors of the ABA signaling network in different conditions. Furthermore, the results obtained for the ABA system can enable experimentalists to rapidly rank and test different hypotheses about stomatal closure. The combination of methods presented here can be readily applied to other biological networks as well.

2. Boolean network models

Boolean network models are qualitative representations of a system in which nodes are different components of the system and edges represent interactions and processes among them. Boolean models of biological regulatory networks such as the ABA

signal transduction network contain directed edges. The state of each node is described by a binary variable, where a value of 1 represents that the node is ON (active), and a value of 0 denotes that it is OFF (inactive). Let i ($i=1, \ldots, N$) represent the nodes of a regulatory network with N nodes. The basic assumption of Boolean models is that the state of each node i at any time instant t, $X_i(t)$, is determined by the states of other nodes in the system (input nodes) at previous time instants through a Boolean function (rule). This function is a logical statement that acts on the previous states of the input nodes via the Boolean operators 'and', 'or', and 'not'. In order to compute $X_i(t)$, it is necessary to specify the implementation of time (including what exactly "previous" means). In this direction, different techniques have been proposed in the literature. In the simplest implementation, called synchronous model (Kauffman, 1993), the state of all nodes of the network is updated at the same time. More precisely,

$$X_i(t+1)=F_i(X_1(t),\ldots,X_N(t)) \quad \forall\, i=1,2,\ldots,N \tag{1}$$

where F_i is the Boolean function associated with node i. Synchronous models are deterministic, meaning that if the system starts at a given initial condition it always converges to the same state after the same number of time steps (Kauffman, 1993). Since the total number of states that a network of N nodes can have is finite (i.e., 2^N), after a large enough number of time steps, the system must necessarily return to a previously visited state. This implies the emergence of an attractor in the state space of the system, which can be in the form of either a single state (fixed point), or a repeating sequence of states (limit cycle). The length (period) of a limit cycle is the number of states in the cycle. The basin of attraction of an attractor is defined as the set of all states that if chosen as the initial states of the system, will lead to that attractor. In synchronous Boolean models the basins of attraction of different attractors do not intersect (Kauffman, 1993). The fixed points of a Boolean system can be determined by taking away the time-dependence of the update functions and solving the resulting set of equations.

Although the synchronous model has been widely used due to its simplicity and ease of implementation, it fails to consider the variety of time scales associated with different types of processes possible in a given biological system (Papin et al., 2005). To address this drawback, asynchronous models (Thomas, 1973) were developed in which different nodes are updated based on their specific time scales. However, since the actual durations of specific biological processes are not usually known, most of the asynchronous algorithms employ a random updating scheme. For example, in the random order asynchronous (ROA) algorithm (Chaves et al., 2005; Harvey and Bossomaier, 1997; Li et al., 2006; Thakar et al., 2007; Zhang et al., 2008) it is assumed that each node in the network is updated exactly once during each time unit (round of update). In this algorithm an updating order is randomly assigned to the nodes of the network at each round of update. Consider updating a network with N nodes at the $(t+1)$th time unit, given that the states of all nodes at all previous time points are already known. First, a random permutation of $\{1, \ldots, N\}$, say $P=(P_1, \ldots, P_N)$ is generated. Then the state of node i, the P_ith node that should be updated, at time $t+1$ can be obtained as follows (Chaves et al., 2005):

$$X_i(t+1)=F_i(X_1(\tau_{1,t}),\ldots,X_N(\tau_{N,t})) \quad \forall\, i=1,2,\ldots,N \tag{2}$$

where

$$\tau_{j,t}=\begin{cases} t & \text{if} \quad P_j>P_i \\ t+1 & \text{if} \quad P_j<P_i \end{cases}$$

meaning that if the input node j has been last updated in the tth round, then $X_j(t)$ should be used in the right hand side of Eq. (2), while if it has been already updated in the $(t+1)$th round, then $X_j(t+1)$ should be used.

The two other asynchronous methods that we will consider are the general asynchronous (GA) (Harvey and Bossomaier, 1997) and deterministic asynchronous (DA) (Chaves et al., 2006) approaches. In the GA model, at each time step a randomly selected node is updated. In this approach it is quite possible that a node chosen in the current time step will be selected again in the subsequent time step. Note that the time unit of the GA model is the $(1/N)$th of the time unit of the ROA model. In the DA model, each node i is associated with a pre-selected time unit γ_i (usually a multiple of the time step), and is updated at times $t=k\gamma_i$ for any positive integer k. More specifically,

$$X_i(t+1)=\begin{cases} F_i(X_1(t),\ldots,X_N(t)) & \text{if} \quad t+1=k\gamma_i, \quad k=1,2,\ldots \\ X_i(t) & \text{otherwise} \end{cases} \tag{3}$$

The randomness of the ROA and GA Boolean models implies that the resulting attractors can be different from the attractors of deterministic models. Fixed points, being time-independent, are identical to their deterministic counterparts, but for limit cycles there are no such clear counterparts (Harvey and Bossomaier, 1997). Instead of limit cycles, a new kind of attractor appears in these random asynchronous models, named *loose attractor* by Harvey and Bossomaier (1997). According to their definition, an attractor A is called a loose attractor if for all possible states S of the state space of the network belonging to A, all possible successor states of S also belong to A. In other words, in a loose attractor, the system's trajectory travels irregularly over a set of states. As Harvey and Bossomaier (1997) stated, a loose attractor is equivalent to a strongly connected component (a set of nodes for which there is a directed path between any pair of them) of the directed graph formed by the state transitions in the system. However, this correspondence of the loose attractors, as defined above, to the strongly connected components (SCCs) is not true in general, as it holds only if the out-component of the SCC (the set of states that can be reached from the SCC) is an empty set. Thus in the following we will define the loose attractors as SCCs with a null out-component in the state transition graph of the system. Other terminologies for loose attractors used in the recent literature are complex loops (Garg et al., 2008) and terminal SCCs (Faure et al., 2006). Harvey and Bossomaier (1997) also defined the *definite basin of attraction* of a loose attractor as the set of states from which all possible paths lead into that attractor, and the *possible basin of attraction* as the set of states from which at least one possible path leads into the definite basin of attraction. This possible basin of attraction corresponds to the in-component (the set of states that can reach the SCC) of the SCC of the state transition graph. Note that since no randomness is involved in the DA model, the transition graph obtained by this method may have limit cycles as in the synchronous model.

There has been a significant interest in relating the structure of regulatory networks, specifically the existence of positive and negative feedback loops, to their dynamical properties (Sontag et al., 2008). It has been conjectured that the existence of a positive feedback loop in the regulatory network is a necessary condition for the existence of several stable fixed points in the dynamics (multistability), whereas a negative feedback loop is necessary for observing sustained oscillations (Thomas, 1981; Thomas and D'Ari, 1990). There have been several efforts towards proving these hypotheses in both a continuous framework (Cinquin and Demongeot, 2002; Gouze, 1998) as well as a discrete framework (Reichard and Comet, 2007; Remy et al., 2008). A few recent works provide a sufficient condition for Thomas' conjectures in a discrete framework (Remy and Ruet, 2008; Siebert, 2009). As the ABA signal transduction network contains both

positive and negative feedback loops, it has the potential for both multistability and sustained oscillations; unfortunately the sufficient condition cannot be directly applied in this case.

The exponential dependence of the state space on the number of nodes poses a substantial obstacle to mapping the state transitions of even relatively small (above ten-node) networks. Here we propose and implement two ways in which the state space can be reduced without significant loss of information. Most Boolean networks, and especially Boolean models of signal transduction networks with a steady signal, contain nodes whose state stabilizes in an attracting state after a transient period, whether or not the system as a whole has a fixed point attractor. The attracting states of these nodes can be quickly figured out by an inspection of their Boolean updating functions. As the stabilization depends on the Boolean rules only, different asynchronous methods can only differ in the duration of the transient period. Therefore we concentrate on the dynamics of the sub-network consisting of only those nodes with non-stationary behavior, and use the steady states of the stationary nodes in the Boolean rules governing the state transitions of the fluctuating nodes. As a second simplification, we collapse equivalent nodes and edges in the network to reduce it to a size with a manageable state space. This way we obtain complementary views on the same system: a complete dynamical description of a topologically reduced version and a qualitative or partial analysis of the complete network. The computer simulations for this study have been implemented in python using the open source software packages BooleanNet (Albert et al., 2008) (available at http://code.google.com/p/booleannet/) and NetworkX (available at http://networkx.lanl.gov/).

3. Results

The experimental results concerning ABA-induced stomatal closure have been compiled into a network by Li et al. (2006) (see Fig. 1). This network contains 54 nodes of which the state of 39 is regulated by other nodes (Li et al., 2006). ABA serves as the input node of this network, whereas Closure is considered as the output node. The edges represent interactions between two nodes, where an arrowhead/short segment at the end of an edge denotes activation/inhibition. Furthermore, a predictive dynamic model of the process was developed by Li et al. (2006) by using the ROA Boolean approach. The output of the model was chosen as the percentage of simulations, involving different initial conditions for nodes other than ABA and different update orders, that at a given time step attained state 1 for the node Closure (called the percentage of closure). This study also revealed that certain components of the system, such as Ca_c^{2+}, show oscillatory behavior (Li et al., 2006).

We use the same Boolean rules as Li et al. (2006) in our study. We assume that the unregulated nodes included in the Boolean rules, such as ABA, are in the ON state. Based on this assumption, and using Boolean algebra, the Boolean functions of many nodes can be simplified. As a result, the majority of the regulated nodes of the network (26 out of 39) stabilize in an ON or OFF state within eight time steps with the synchronous method and within eight rounds of update in the ROA method. In particular, the node Closure stabilizes in the ON state. Subsequently, we concentrate on the dynamics of the sub-network consisting of only those nodes with oscillatory behavior, and use the steady states of the stationary nodes in the Boolean rules governing the state transitions of the oscillating nodes. Li et al. (2006) observed sustained fluctuations during the period of their study which consisted of ten rounds of update in the ROA model. Here, we aim to determine whether the oscillatory behavior is sustained in the long-time behavior and whether it constitutes an attractor of the state space of the system for the ROA, GA, and DA models.

The sub-network comprising only oscillatory nodes contains 13 nodes as illustrated in Fig. 2. The Boolean rules governing the state of the nodes in this sub-network are given in Table 1. Although this simplified network has a size considerably smaller than the original network, it is still computationally taxing to map the state trajectories of the network, especially for the asynchronous models, due to the combinatorial nature of the underlying problem. Therefore, we iteratively simplified the 13-node network into smaller sub-networks to obtain a general insight into the dynamics of the system. As a first simplification, we removed the nodes KEV and KAP, which have no regulatory effects on the other nodes of the sub-network. From here on, we refer to the 13-node sub-network without these two nodes as the 11-node sub-network. In the following sections, we discuss the results of the synchronous and three asynchronous models for this sub-network and its variants.

3.1. Synchronous model

We found by simulation that with synchronous update, the 11-node sub-network possesses three attractors: a fixed point in which all the 11 nodes are in the OFF state (we will call such a fixed point a null fixed point) and two distinct limit cycles of period four as given in Table 2. The fixed point is reachable from 27 ($\sim$1%) out of 2048 possible initial conditions. The basin of attraction of the first limit cycle contains 426 states ($\sim$21% of all the initial states) whereas that of the second cycle is comprised of 1595 initial states ($\sim$78% of all the initial states). The two limit cycles contain markedly different levels of node activation as the frequency of the ON state for each node in the second limit cycle is double of the corresponding frequency in the first one (see Table 2). Interestingly, we observe that the basin of attraction of the three attractors is an increasing function of the frequency of the ON states in the attractor.

In addition to the numerical simulations, we also performed a theoretical analysis using scalar equations to determine the attractors of the synchronous model. Scalar equations and reduced scalar equations have been previously found to be useful in acquiring information about the cyclic and transient structure of synchronous Boolean networks (Farrow et al., 2004; Heidel et al., 2003). As defined by Heidel et al. (2003), a *scalar equation* is an ordinary recurrence equation for a particular node of a Boolean network. However, sometimes such equations may take an impractically complex form. To tackle this difficulty, a simpler form called reduced scalar equation (Farrow et al., 2004) can be derived by further iterating the original recurrence relationship. In order to obtain the scalar equations for the 11-node sub-network, we first recapitulate all the Boolean rules given in Table 1 as a function of Ca_c^{2+} (see Table 3). The reduced scalar equation corresponding to the node Ca_c^{2+} can then be obtained as below (see Appendix A for details):

$$Ca_c^{2+}(t+8) = Ca_c^{2+}(t+4) \quad (4)$$

Similar equations can be obtained for other nodes of the sub-network. Eq. (4) provides immediate information about the cyclic and transient structure of the network. Considering Eq. (4) and noting the fact that the Boolean functions of all other nodes depend on Ca_c^{2+}, the only possible cycles of the sub-network are of length one, two or four. We find that limit cycles of length two are not possible. To demonstrate this, let us assume that Ca_c^{2+} admits a cycle of length two. Then for sufficiently large t, we have $Ca_c^{2+}(t)=Ca_c^{2+}(t+2k)$ for any positive integer k. But then the Boolean function of the node Ca_c^{2+} (given in Table 3) can be simplified as $Ca_c^{2+}(t)=Ca_c^{2+}(t)$ and [not $Ca_c^{2+}(t)$]. The only

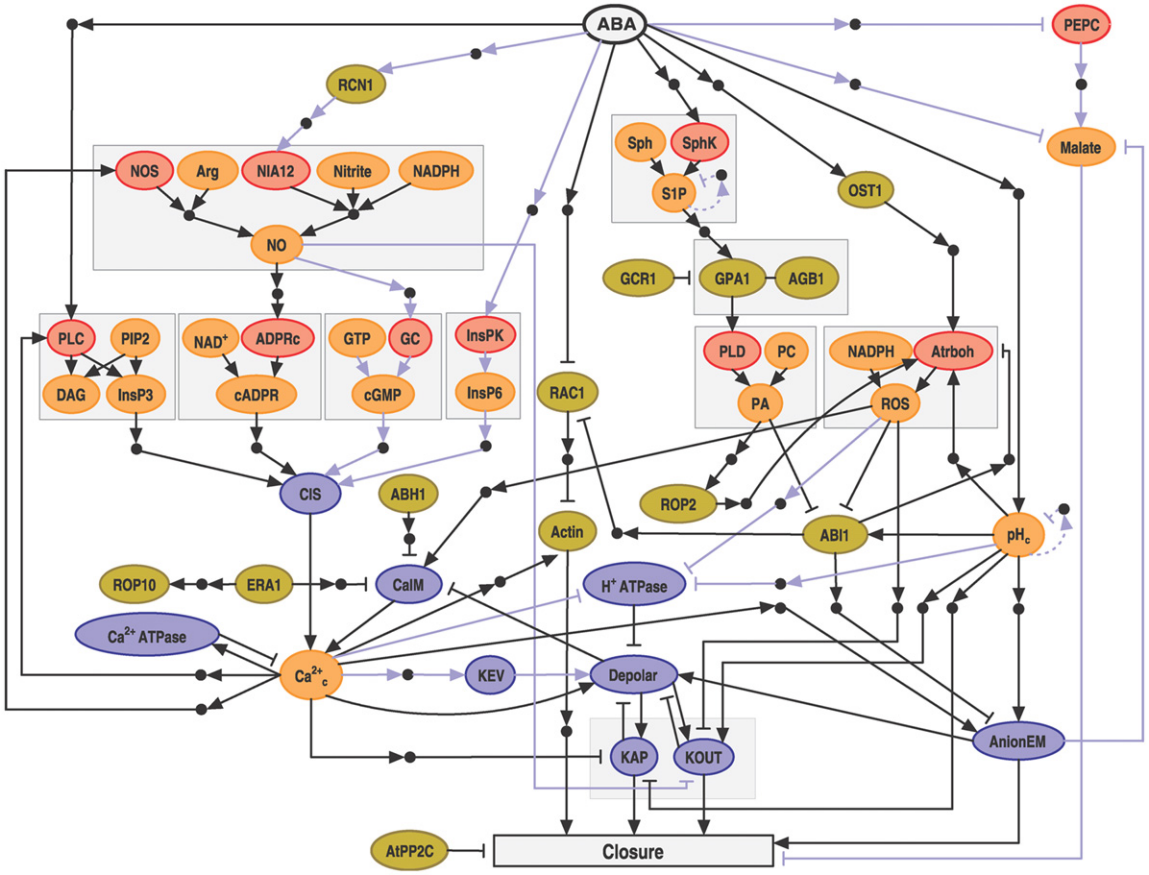

Fig. 1. Guard cell ABA signal transduction network as synthesized in Li et al. (2006). The functions of the nodes are color coded in this figure: enzymes are shown in red, signal transduction proteins are green, membrane transport-related nodes are blue and secondary messengers and small molecules are orange. Small black filled circles represent putative intermediaries of indirect regulatory interactions. Arrowheads represent activation and short perpendicular bars indicate inhibition. Nodes involved in the same metabolic pathway or protein complex are bordered by a grey box. The full names of selected network components corresponding to each abbreviated node label are: ABA, abscisic acid; ABI1, protein phosphatase 2C ABI1; AGB1, heterotrimeric G protein β subunit; AnionEM, anion efflux at the plasma membrane; CaIM, Ca^{2+} influx across the plasma membrane; Ca^{2+}ATPase, Ca^{2+}ATPases and Ca^{2+}/H^+ antiporters responsible for Ca^{2+} efflux from the cytosol; Ca_c^{2+}, cytosolic Ca^{2+} increase; cADPR, cyclic ADP-ribose; cGMP, cyclic GMP; CIS, Ca^{2+} influx to the cytosol from intracellular stores; Depolar, plasma membrane depolarization; GC, guanyl cyclase; GCR1, putative G protein-coupled receptor; H^+ATPase, H^+ATPase at the plasma membrane; InsP3, inositol-1,4,5-trisphosphate; KEV, K^+ efflux from the vacuole to the cytosol; KOUT, K^+ efflux through slowly activating outwardly rectifying K^+ channels at the plasma membrane; NOS, nitric oxide synthase; NO, nitric oxide; PA, phosphatidic acid; PLC, phospholipase C; S1P, sphingosine-1-phosphate (Li et al., 2006). (For interpretation of the references to colour in this figure legend, the reader is referred to the web version of this article.)

solution of this equation implies that Ca_c^{2+} stabilizes in the OFF state, but that gives the fixed point of the network, not a cycle of length two. Therefore, the sub-network can only have fixed points or cycles of length four, confirming the results obtained by simulations.

A similar argument can be used to prove that the sub-network possesses a single fixed point, namely the null fixed point. To obtain the cycles of length four, we should have $Ca_c^{2+}(t+4) = Ca_c^{2+}(t)$ for large enough t, which simplifies the Boolean function of the node Ca_c^{2+} (given in Table 3) as follows:

$$Ca_c^{2+}(t+2) = Ca_c^{2+}(t+2) \text{ and } [\text{not } Ca_c^{2+}(t)] \quad (5)$$

Based on this equation state 1 for Ca_c^{2+} at time instant t implies state 0 for this node at time instant $t+2$. Therefore the state of Ca_c^{2+} is on one of the orbits (0, 0, 0, 0), (1, 0, 0, 0) or (1, 1, 0, 0). The first orbit implies that Ca_c^{2+} stabilizes in the OFF state, which gives us the null fixed point found before. Considering the last two orbits and using the Boolean functions indicated in Table 3, we obtain the limit cycles of length four obtained by simulations (see Table 2). Furthermore, using Eq. (4) and similar equations for other nodes in the 11-node sub-network, the longest possible transient trajectory of the sub-network is found to be of length nine. In other words, given any point in the state space of the sub-network, after at most nine iterations it will reach either the null fixed point or one of the two limit cycles. Numerical simulations of this sub-network indicate that the actual longest transient trajectory is of length seven. In effect, though certain nodes' phase follows Ca_c^{2+} with a delay during the cycle, their transient is shorter than the sum of the transient of Ca_c^{2+} and the corresponding delay. We also verified analytically that the basin of attraction of the fixed point contains 27 states.

It should be noted that adding back the two nodes KEV and KAP (see Fig. 2) does not change the attractors of the network. More precisely, the system still possesses a fixed point and two limit cycles of length four, in which the states of the nodes KEV and KAP are determined by Ca_c^{2+}. Considering the attractors for the 13-node sub-network together with those nodes that were already considered to be in their steady state, we conclude that the synchronous model of the whole ABA signal transduction network eventually settles into either a fixed point or one of the two limit cycles of length four.

3.2. Random order asynchronous (ROA) model

To be able to handle the additional state transitions possible in asynchronous models, we further simplified the 11-node sub-network. This sub-network has three different positive

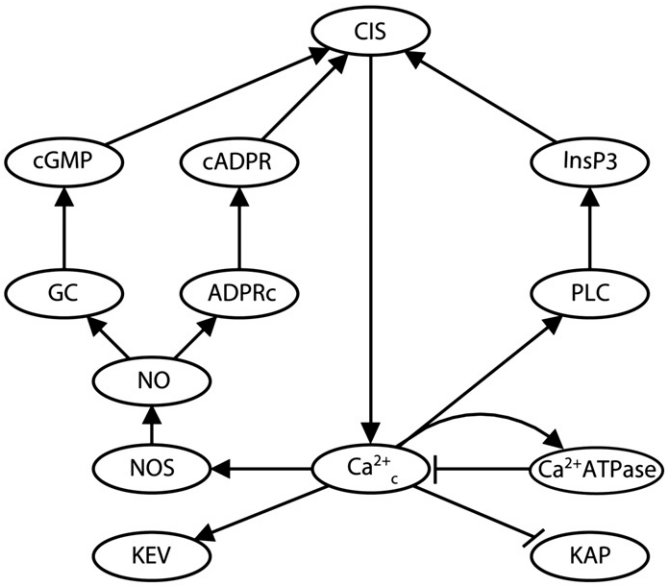

Fig. 2. The 13-node sub-network of the guard cell ABA signal transduction network obtained by removing the nodes that stabilize within eight time steps. The node labels are the same as in Fig. 1. The 11-node sub-network is derived from this network by removing the nodes KEV and KAP.

Table 1
Boolean rules governing the state of the 13-node sub-network depicted in Fig. 2. For simplicity, the nodes' states are represented by the node names. The symbol* indicates the future state of the marked node.

Node	Boolean rule
NOS	$NOS^*=Ca_c^{2+}$
NO	$NO^*=NOS$
GC	$GC^*=NO$
ADPRc	$ADPRc^*=NO$
cADPR	$cADPR^*=ADPRc$
cGMP	$cGMP^*=GC$
PLC	$PLC^*=Ca_c^{2+}$
InsP3	$InsP3^*=PLC$
CIS	CIS*=(cGMP and cADPR) or InsP3
Ca^{2+}ATPase	$Ca^{2+}ATPase^*=Ca_c^{2+}$
Ca_c^{2+}	Ca_c^{2+} *=CIS and (not Ca^{2+}ATPase)
KAP	$KAP^*=$not Ca_c^{2+}
KEV	$KEV^*=Ca_c^{2+}$

Table 2
The limit cycles observed in the synchronous model for the 11-node sub-network given in Fig. 2.

NOS	NO	GC	ADPRc	cADPR	cGMP	PLC	InsP3	CIS	Ca^{2+}ATPase	Ca_c^{2+}
(a) The first limit cycle										
1	0	0	0	0	0	1	0	1	1	0
0	1	0	0	0	0	0	1	0	0	0
0	0	1	1	0	0	0	0	1	0	0
0	0	0	0	1	1	0	0	0	0	1
(b) The second limit cycle										
1	1	0	0	0	0	1	1	1	1	0
0	1	1	1	0	0	0	1	1	0	0
0	0	1	1	1	1	0	0	1	0	1
1	0	0	0	1	1	1	0	1	1	1

feedback loops involving Ca_c^{2+} and CIS, as well as a negative feedback loop made up of Ca_c^{2+} and Ca^{2+}ATPase. Thus the essence of this network is captured by only three nodes, Ca_c^{2+}, Ca^{2+} ATPase, and CIS, forming a coupled positive and negative feedback loop. Fig. 3(a) shows this 3-node sub-network with the corresponding Boolean rules. We have analytically determined the state transition graph of this sub-network (see Fig. 3(b)). The digits of the binary numbers in this figure indicate the state of the nodes in the order CIS, Ca_c^{2+}, and Ca^{2+}ATPase. For example, the binary sequence 001 represents CIS=OFF, Ca_c^{2+}=OFF, and Ca^{2+}ATPase=ON. As can be seen in Fig. 3(b), the system has a fixed point to which all the states converge. This null fixed point, in which all the three nodes are in the OFF state, can be also obtained by solving the time-independent Boolean equations.

Table 3
The alternative statement of the Boolean rules governing the state of the synchronous model of the 11-node sub-network given in Fig. 2 as a function of Ca_c^{2+}.

Node	Boolean rule
NOS	$NOS(t+1)=Ca_c^{2+}(t)$
NO	$NO(t+2)=Ca_c^{2+}(t)$
GC	$GC(t+3)=Ca_c^{2+}(t)$
ADPRc	$ADPRc(t+3)=Ca_c^{2+}(t)$
cADPR	$cADPR(t+4)=Ca_c^{2+}(t)$
cGMP	$cGMP(t+4)=Ca_c^{2+}(t)$
PLC	$PLC(t+1)=Ca_c^{2+}(t)$
InsP3	$InsP3(t+2)=Ca_c^{2+}(t)$
CIS	$CIS(t+5)=Ca_c^{2+}(t)$ or $Ca_c^{2+}(t+2)$
Ca^{2+}ATPase	$Ca^{2+}ATPase(t+1)=Ca_c^{2+}(t)$
Ca_c^{2+}	$Ca_c^{2+}(t+6)=[Ca_c^{2+}(t)$ or $Ca_c^{2+}(t+2)]$ and [not $Ca_c^{2+}(t+4)]$

We determined that the transition matrix corresponding to the state space of the 3-node sub-network is as follows:

$$P=\begin{pmatrix} 1 & 0 & 0 & 0 & 0 & 0 & 0 & 0 \\ 1 & 0 & 0 & 0 & 0 & 0 & 0 & 0 \\ 1/3 & 1/6 & 0 & 0 & 0 & 1/3 & 0 & 1/6 \\ 1/3 & 1/6 & 0 & 0 & 1/6 & 1/3 & 0 & 0 \\ 1/2 & 0 & 0 & 0 & 0 & 0 & 1/6 & 1/3 \\ 5/6 & 0 & 0 & 0 & 0 & 0 & 1/6 & 0 \\ 0 & 1/6 & 0 & 0 & 0 & 1/3 & 0 & 1/2 \\ 1/3 & 1/6 & 0 & 0 & 1/6 & 1/3 & 0 & 0 \end{pmatrix}$$

where each entry of the matrix, p_{ij}, denotes the probability of going from state i to state j for $0 \le i,j \le 7$ (the numbers 0–7 are the decimal representation of the binary numbers given in Fig. 3(b)). In other words, the probabilities p_{ij} are the fractions of the total number of update orders (i.e. permutations) causing a change of state from i to j in one step. It should be noted that the matrix P is a stochastic matrix, because $0 \le p_{ij} \le 1$ for $0 \le i,j \le 7$, and all rows sum up to one. In the sense of a *Markov chain*, the fixed point of the system is an *absorbing state*, i.e., a state left unchanged in all permutations. All other states are *transient states* because there is a positive probability that the chain does not return to these states after leaving them. Hence the vector $\pi=(1,0,0,0,0,0,0,0)$ is the stationary distribution of the chain where each component $\pi_i\,(0 \le i \le 7)$ denotes the long-term probability of being in state i.

The strongly connected component (SCC) of the state space in Fig. 3(b) contains half of the total states, namely states 100, 101, 110, and 111 (see symbols with a grey background in Fig. 3(b)). However, every state, including those in the SCC, is connected to the fixed point (i.e., it is in the in-component of the fixed point), implying that every state trajectory will ultimately converge to the fixed point. An immediate calculation, using the transition matrix P, shows that the average probability of reaching the fixed

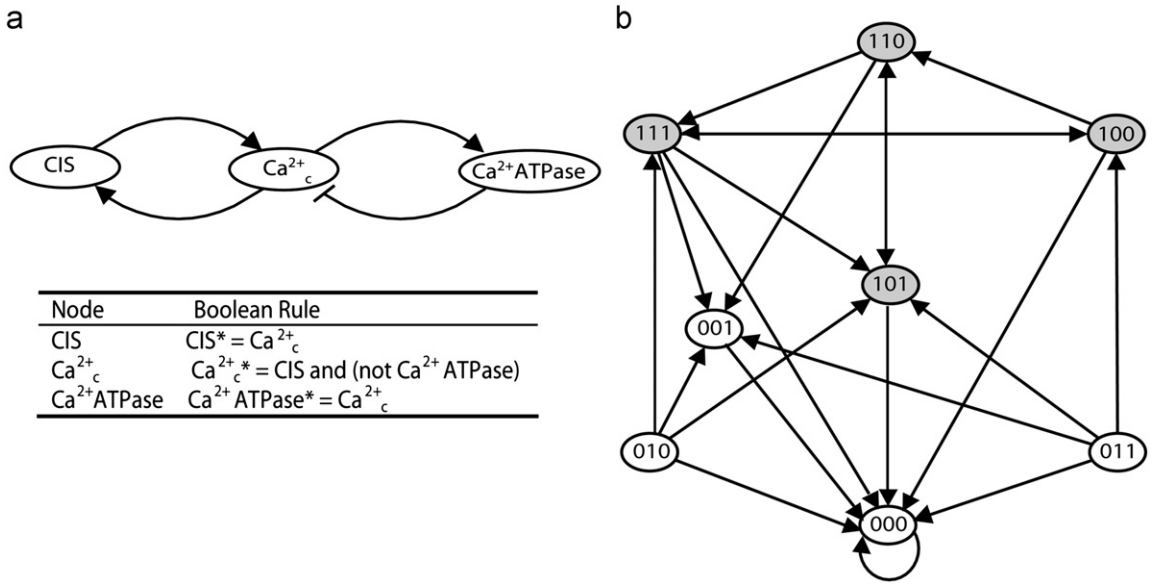

Fig. 3. The 3-node sub-network formed by the nodes CIS, Ca^{2+}_c, and Ca^{2+}ATPase with the corresponding state transition graph. (a) The 3-node sub-network and the Boolean functions governing the state of the nodes in the sub-network. (b) The state transition graph of the 3-node network given in (a) obtained from the ROA model. The binary numbers in each node represent the states of the three-node system in the order CIS, Ca^{2+}_c and Ca^{2+}ATPase, and a directed edge between two states indicates that the second state can be obtained from the first after a round of update of the nodes' states. The four nodes whose symbols have a grey background form the strongly connected component of the state transition graph.

Table 4
The expected number of time steps for absorbing into the fixed point when the Markov chain corresponding to the 3-node sub-network given in Fig. 3(a) starts from the transient states in the ROA model.

State	001	010	011	100	101	110	111
Absorption time	1.00	1.98	2.00	2.10	1.44	2.65	2.00

point in one step is larger than the average probability of remaining in the SCC for one step. We also estimated the expected times for absorption into the fixed point (Tuchwell, 1988) when the chain starts from each of the transient states (see Table 4). As given in this table, the absorption time for state 001 is less than that for other states since it can reach the fixed point in only one step (see Fig. 3(b)). In addition, we can see that state 101 in the SCC has a shorter absorption time compared to the other states in the SCC because with a probability of 5/6 it reaches the fixed point in one step. In summary, this network does not support sustained oscillations as an attracting behavior.

In the next step, we considered a larger sub-network to see whether the same behavior is observed. As can be seen in Fig. 2, in the 11-node sub-network there are two different paths from NO to CIS with the same length. The two paths are conditional on each other, as both cGMP and cADPR need to be ON in order to activate CIS, thus for simplification we collapsed these two equivalent paths into one. We next removed the node cGMP from the network which has both in-degree (number of edges entering a node) and out-degree (number of edges coming out of a node) of one and acts as a delay between the two nodes GC and CIS. The resulting 8-node sub-network, which has two positive feedback loops of length four and five, and one negative feedback loop of length two, is depicted in Fig. 4. The Boolean rules governing the state of the nodes of this sub-network are given in Table 5. Since in this case there are two positive feedback loops competing with one negative feedback loop, a loose attractor may be possible.

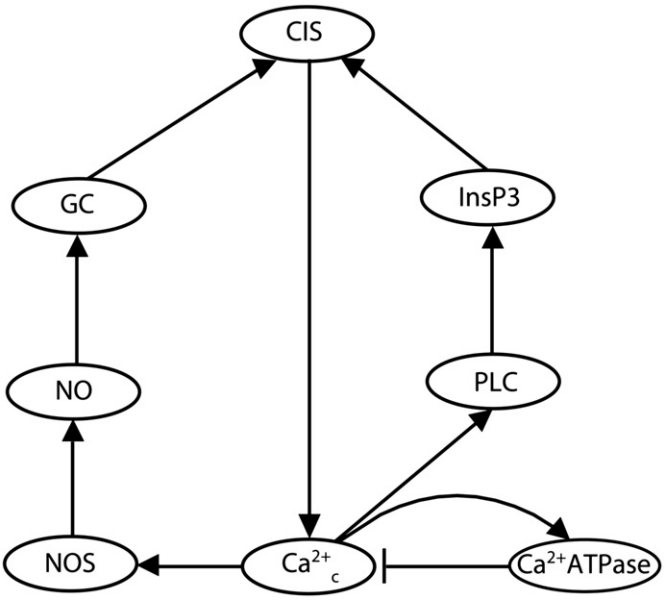

Fig. 4. The 8-node sub-network obtained by collapsing the two paths from NO to CIS and eliminating the node cGMP in the 11-node sub-network (see Fig. 2).

We numerically probed the dynamics of this sub-network and found that the majority of the nodes of the state space (237 out of 256) are part of a giant SCC. The average in-degree of the SCC is

Table 5
The Boolean rules governing the state of the 8-node sub-network represented in Fig. 4.

Node	Boolean rule
NOS	NOS*=Ca_c^{2+}
NO	NO*=NOS
GC	GC*=NO
PLC	PLC*=Ca_c^{2+}
InsP3	InsP3*=PLC
CIS	CIS*=GC or InsP3
Ca^{2+}ATPase	Ca^{2+}ATPase*=Ca_c^{2+}
Ca_c^{2+}	Ca_c^{2+} *=CIS and (not Ca^{2+}ATPase)

equal to 32 and its average out-degree is 31, thus the SCC is densely connected. The fixed point of the system is still the null fixed point, in which all the nodes are in the OFF state. The large in-degree of the fixed point (242) shows that almost all the nodes of the state space can reach the fixed point in one step. By extension of the results obtained for the 8-node sub-network, we can conclude that the whole 11-node sub-network under ROA update the only attractor of the system is the null fixed point.

We also investigated whether small changes to the Boolean rules or to the topology of the 8-node sub-network can strengthen the strongly connected component of the state transition graph (see Appendix B for details) and found that no such changes can strengthen it to the point of becoming a loose attractor.

In summary, based on the results we discussed for the simplified sub-networks, we can conclude that the ROA model of the ABA signal transduction network possesses only a fixed point, which is identical to the fixed point of the synchronous model. It is important to notice the difference between the basin of attraction of the attractors for the synchronous and ROA approaches. In the synchronous method the limit cycles had the majority of the states in their basins of attraction, whereas, in the asynchronous case all the states are in the definite basin of attraction of the fixed point. This result is consistent with previous reports that synchronous Boolean models can have spurious oscillations (Faure et al., 2006; Mochizuki, 2005). For example, a comparison of synchronous Boolean and continuous models of gene networks has showed that many of the periodic oscillations observed in the Boolean model were not present in the continuous model (Mochizuki, 2005).

3.3. General asynchronous (GA) model

For this asynchronous model, we analytically determined the state transition graph corresponding to the simplified 3-node sub-network given in Fig. 3(a). As represented in Fig. 5, the state 000 serves as the fixed point and the SCC of the state transition graph contains the same four states as that of the ROA model. However, there are some important differences between the transition graphs of the GA and ROA models. First, the GA graph (Fig. 5) has fewer edges than the ROA graph (Fig. 3(b)). This is explained by the fact that only one node can change state during a GA update, compared to all three potentially changing states during an ROA round of update, thus the number of states adjacent to a given state is less in the GA model than in the ROA model. Second, there are more self loops in Fig. 5 than in Fig. 3(b) since it is quite possible in the GA model that updating a particular node does not change the state of the system. Finally, in Fig. 3(b) almost all the states can reach the fixed point in one step,

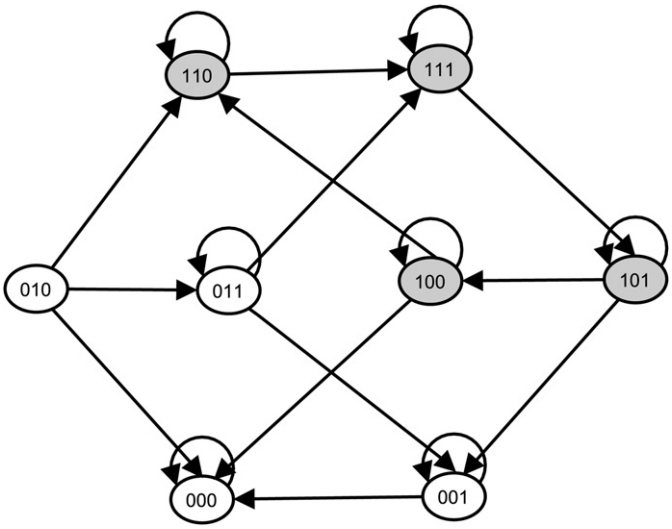

Fig. 5. The state transition graph of the 3-node sub-network given in Fig. 3(a) obtained from the GA model. The binary numbers in each node represent the states of the 3-node system in the order CIS, Ca_c^{2+}, and Ca^{2+}ATPase, and a directed edge between two states indicates that the second state can be obtained from the first after a time step. The four nodes whose symbols have a grey background form the strongly connected component of the state transition graph.

Table 6
The expected number of time steps for absorbing into the fixed point when the Markov chain corresponding to the 3-node sub-network starts from the transient states in the GA model.

State	001	010	011	100	101	110	111
Absorption time	3	8	8	8	7	13	10

which is not the case in the GA model. The transition matrix corresponding to the GA graph is as following:

$$P=\begin{pmatrix} 1 & 0 & 0 & 0 & 0 & 0 & 0 & 0 \\ 1/3 & 2/3 & 0 & 0 & 0 & 0 & 0 & 0 \\ 1/3 & 0 & 0 & 1/3 & 0 & 0 & 1/3 & 0 \\ 0 & 1/3 & 0 & 1/3 & 0 & 0 & 0 & 1/3 \\ 1/3 & 0 & 0 & 0 & 1/3 & 0 & 1/3 & 0 \\ 0 & 1/3 & 0 & 0 & 1/3 & 1/3 & 0 & 0 \\ 0 & 0 & 0 & 0 & 0 & 0 & 2/3 & 1/3 \\ 0 & 0 & 0 & 0 & 0 & 1/3 & 0 & 2/3 \end{pmatrix}$$

Based on the transition matrix we estimated the expected number of time steps for absorption into the fixed point from each of the transient states (see Table 6). A comparison of the absorption times for the ROA and GA models (Tables 4 and 6) shows that all the states have longer absorption times in the GA model than in the ROA model, in agreement with the higher number of self loops in the GA graph.

The ROA and GA state transition graphs are related by a variant of transitive closure: the ROA state transition graph contains an edge for every path of length three (generally, of length N) that represents the update of different network nodes in the GA state transition graph. Since transitive closure and its opposite, transitive reduction, do not change the strongly connected components and their in- and out-components, we expected that the similarity of the ROA and GA models is preserved for the 8-node sub-network shown in Fig. 4 as well. Indeed we found that the 8-node sub-network exhibits a single fixed point, namely the null (all-OFF) state, similar to the ROA model. However, the in-degree of the fixed point is 9 in the GA model which is remarkably

smaller than that obtained with the ROA model (242). Furthermore, we identified a large SCC containing 238 nodes of the state space (out of 256), with average in- and out-degrees of 5 and 4, respectively. The results for changing the Boolean rules or the topology of the 8-node sub-network obtained from these two updating schemes were almost the same and the only difference was related to the average in- and out-degrees (see Appendix B for details). This agreement between the two methods goes beyond the previously observed equality of the expected value of the time taken between two consecutive updates of a node (Schonfisch and de Roos, 1999). Thus we can conclude that the GA model of the ABA signal transduction network possesses only a fixed point, which is identical to the fixed point of the synchronous and of the ROA model.

3.4. Deterministic asynchronous (DA) model

We applied this method of update to the 3-node sub-network represented in Fig. 3(a) with many different choices of time units. In all cases, the sub-network possesses the null fixed point. When the time unit for the node CIS is the largest, interesting additional behaviors are observed. Specifically, in some cases, the four states that formed the SCC of the transition graph in the ROA and GA models now form a limit cycle. The length of the observed limit cycles can vary depending on the frequency of the four states in the limit cycles. As the additional nodes in the 8-node sub-network only affect the effective time units between the three main nodes, there are no dynamical behaviors which are possible in the 8-node sub-network and would not be in the 3-node sub-network. Thus in the following we will only consider the 3-node sub-network.

Let γ_i be the time unit associated with node i, where i is one of the three nodes of the sub-network. In the following, we prove that under some conditions, limit cycles for the DA model exist and we express the length of the limit cycles in terms of γ_i.

Proposition 1. *If* $t_{Ca_c^{2+}} = 2k+1$, *where* k *is a positive integer number,* $t_{Ca^{2+}ATPase} = 2$ *and* $t_{CIS} = 2t_{Ca_c^{2+}}$, *then the transition graph of the* 3*-node sub-network has a limit cycle of length* $t_{Ca_c^{2+}} + 1$.

Proof. First note that if CIS is in the OFF state initially, then the condition $t_{CIS} > t_{Ca_c^{2+}}$ implies that the node Ca_c^{2+} will be turned OFF and therefore the system eventually settles into the null fixed point. Thus, a necessary condition for the basin of attraction of a cycle is that the node CIS must be in the ON state initially. Assuming that, we need to consider two cases:

Case 1: The node Ca_c^{2+} is in the OFF state initially, i.e. the initial state of the system is either 100 or 101 (the order of the nodes in these states is CIS, Ca_c^{2+}, and Ca^{2+}ATPase). Without loss of generality, assume that the initial state is 100. A similar argument with minor changes holds for the case where the system starts from the state 101. The system stays at the state 100 at all even time instants, in which Ca^{2+}ATPase is updated, until the time point $t=2k+1$, when Ca_c^{2+} is updated, and the state of the system changes to 110. Hence, the number of time steps the system stays in the state 100 (without considering the initial state) is $[t_{Ca_c^{2+}}/2] = k$, where $[x]$ is the greatest integer less than or equal to x. At $t=2k+2$, the state of the system changes from 110 to 111 because Ca^{2+}ATPase is updated. The system's state remains unchanged until $t=4k+2=t_{CIS}$, when all the nodes are updated, causing a change of state to 101. Note that the number of time steps that the system visits the state 111, before it reaches the state 101, is again $[t_{Ca_c^{2+}}/2] = k$. Then at $t=4k+4$, Ca^{2+}ATPase is updated and the system returns to the state 100 and the above scenario repeats again. Therefore, the length of the limit cycle is $k+1+k+1 = 2k+2 = t_{Ca_c^{2+}}+1$. Table 7 summarizes this argument.

Case 2: The node Ca_c^{2+} is in the ON state initially, i.e. the initial state of the system is either 110 or 111. Without loss of generality, we can assume that the initial state is 110. At $t=2$, the node Ca^{2+}ATPase is updated and the state of the system changes to 111 and it stays there until the time point $t=2k+1$, when Ca_c^{2+} is updated, and the system's state changes to 101. At $t=2k+2$, the state of the system changes from 101 to 100 due to a change in the state of Ca^{2+}ATPase. The system's state remains unchanged until $t=4k+2=t_{CIS}$, when all the nodes are updated, causing a change of state to 010. Since CIS is turned OFF, after some time the node Ca_c^{2+} will be turned OFF and hence the network ultimately settles into the null fixed point. □

In conclusion, the limit cycle is formed by the states 100, 110, 111, and 101, and the basin of attraction of the limit cycle contains the states 100 and 101. Importantly, the states 111 and 110, although part of the limit cycle, are not part of its basin of attraction, since when they are used as initial conditions the system will converge to the null fixed point. The other four states are also part of the basin of attraction of the fixed point. The state transition graph corresponding to the 3-node sub-network with

Table 7
The state of the 3-node sub-network at different time steps starting from the initial state 100 obtained from the DA model with the time units given in Proposition 1.

Time / node	$t=0$	$t=2$	…	$t=2k$	$t=2k+1$	$t=2k+2$	…	$t=4k+1$	$t=4k+2$	$t=4k+4$
CIS	1	1	…	1	1	1	…	1	1	1
Ca_c^{2+}	0	0	…	0	1	1	…	1	0	0
Ca^{2+}ATPase	0	0	…	0	0	1	…	1	1	0

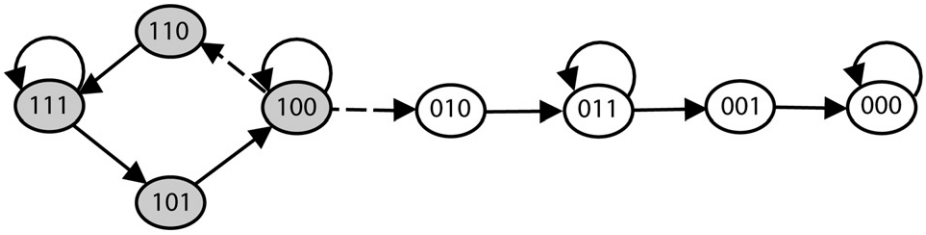

Fig. 6. The state transition graph of the 3-node sub-network for the DA model with the time units given in Proposition 1. The four nodes whose symbols have a grey background form the strongly connected component of the state transition graph. The dash-dotted edges appear only if the system starts from specific initial states: starting from initial state 100 or 101, the system remains in the cycle through the edge from 100 to 110. However, if the system starts from initial state 110 or 111, it reaches the fixed point through the edge from 100 to 010.

the time units specified in Proposition 1 is represented in Fig. 6. The state transition shown as a dash-dotted edge from 100 to 110 is only possible when the system start from initial state 100 or 101. Starting from the other two states in the cycle, the system will converge to the fixed point through the dash-dotted edge from 100 to 010.

Comparing Figs. 3(b) and 6, we observe that the transition graph of the 3-node sub-network for the ROA model is denser than that for the DA model. This is because there are multiple edges coming out of each state in Fig. 3(b) corresponding to different orders of update of the three nodes, while for Fig. 6 there are only three states that have more than one outgoing edge. The self loops present in Fig. 6 but absent from Fig. 3(b) are due to updates in which the state of Ca^{2+}ATPase is updated but does not change; there are no updates of all three nodes that would leave the system's state unchanged unless that state is the null fixed point. There is no direct edge from state 101 to 100 in Fig. 3(b), while there is such an edge in Fig. 6. That is because going from state 101 to 100 requires that the only updated node is Ca^{2+}ATPase, which is impossible in the ROA model but possible in the DA model. Notably, the edges among the nodes in the SCC are the same for the DA and GA models, however the transition graph obtained from the GA model (Fig. 5) is denser and has more self loops than the state transition graph of the DA model.

We have identified four more types of limit cycles. The proof of the following propositions is given in Appendix C:

Proposition 2. *If $t_{Ca_c^{2+}} = 2k$, where k is a positive integer number, $t_{Ca^{2+}ATPase} = 2$ and $t_{CIS} = 2t_{Ca_c^{2+}}$, then the transition graph of the 3-node sub-network has a limit cycle of length $t_{Ca_c^{2+}}$.*

The state transition graph corresponding to this proposition has the same cycle as the state transition graph of Proposition 1, and the limit cycle contains the states on this cycle. The basin of attraction of the limit cycle contains the states 100 and 101 as in Proposition 1. The self loops appear when Ca^{2+}ATPase is updated but its state does not change.

Proposition 3. *If $t_{Ca^{2+}ATPase} = 2k+1$, where k is a positive integer number, $t_{Ca_c^{2+}} = 2$ and $t_{CIS} = 2t_{Ca^{2+}ATPase}$, then the transition graph of the 3-node sub-network has a limit cycle of length $t_{Ca^{2+}ATPase}+1$.*

Proposition 4. *If $t_{Ca^{2+}ATPase} = 2k$, where k is a positive integer number, $t_{Ca_c^{2+}} = 2$ and $t_{CIS} = 2t_{Ca^{2+}ATPase}$, then the transition graph of the 3-node sub-network has a limit cycle of length $t_{Ca^{2+}ATPase}$.*

The transition graph obtained from the conditions mentioned in the last two propositions has the cycle as in Fig. 6 except that the self loops are on the states 101 and 110 where the node Ca_c^{2+} is updated. The tail going out of the cycle to the fixed point is different from Fig. 6. The limit cycle contains the same states as in Propositions 1 and 2, but the basin of attraction of the limit cycle differs in one state, containing the states 101 and 111.

Proposition 5. *If $t_{Ca_c^{2+}} = t_{Ca^{2+}ATPase} = 1$ and $t_{CIS}=4k$, where k is a positive integer, then the transition graph of the 3-node sub-network has a limit cycle of length four.*

The transition graph corresponding to Proposition 5 has the same cycle as in Fig. 6. There is no self loop in this case as the length of the cycle is four, and the tail going out of the cycle to the fixed point differs from that represented in Fig. 6. The basin of attraction of the limit cycle contains the states 101 and 111.

Comparing Propositions 1–5, we find that the corresponding limit cycles share a common sequence of node updates. For each state transition along the cycle, there is one node whose update is required in order for the state transition to occur, and there may be other nodes that can also be updated but do not change state. The nodes that must be updated are: Ca^{2+}ATPase for 101 going into 100, Ca_c^{2+} for 100 going into 110, Ca^{2+}ATPase for 110 going into 111, and Ca_c^{2+} for 111 going into 101. The additional nodes that can be updated are: Ca_c^{2+} for 101 going into 100, Ca^{2+}ATPase for 100 going into 110, Ca^{2+} and CIS for 110 going into 111, and Ca^{2+}ATPase and CIS for 111 going into 101. This suggests that any other time units that lead to the required updates and all or part of the allowed additional updates will lead to a limit cycle.

3.5. Node perturbations

Li et al. (2006) reported that perturbations in S1P, PA, pH_c or four other nodes lead to a reduced closure probability due to fluctuations in the state of the node Closure. With knocking out the nodes AnionEM, Depolar or Actin the system exhibits insensitivity to ABA, i.e., a zero probability for closure. Disruption of ABI1 or Ca^{2+}ATPase results in ABA hypersensitivity, whereas, perturbation in Ca_c^{2+} or two other nodes leads to ABA hyposensitivity, meaning that curve giving the time course of reaching 100% of closed stomata is above (for hypersensitivity), or below (for hyposensitivity) that in the wild type (Li et al., 2006). We further investigate the effect of disrupting (setting in the OFF state) S1P, PA, AnionEM, ABI1, Ca_c^{2+} and pH_c on the attractors of the network. A detailed description of the results for the first five disruptions is given in Appendix D. Here we present the pH_c disruption and summarize the results.

With perturbation in pH_c, 20 nodes stabilize at early steps, leaving a fluctuating sub-network of 19 nodes (see Fig. 7(a) with the Boolean rules in Table 8). Solving the Boolean equations given in Table 8 (independently of time), we found that this sub-network does not have a fixed point, implying that it must have at least one limit cycle for the synchronous method and a loose attractor for the ROA or GA method. Considering the high number of nodes, which makes it computationally inefficient to map the state transition graph, we simplified the sub-network by collapsing a number of redundant paths as shown in Fig. 7(b). We collapsed the 11-node sub-graph common to Figs. 2 and 7(a) into the simple 3-node sub-graph of Fig. 3(a). Then, we merged the parallel positive paths between Ca_c^{2+} and Depolar into a single edge, and eliminated three nodes. We also consolidated the two positive paths from Depolar to Closure into one, and removed the node KAP from the network. The Boolean functions governing the state of the resulting 7-node sub-network (represented in Fig. 7(b)) are listed in Table 9. We confirmed by solving the Boolean equations given in Table 9 that this simplified sub-network maintained the original's lack of fixed point.

Numerical simulations revealed that with synchronous updating the transition graph of the 7-node sub-network has a limit cycle of length five (see Table 10) having all the states in its basin of attraction. For the ROA (or the GA) method, the transition graph of the sub-network given in Fig. 7(b) has a loose attractor containing the majority of the states (120 out of 128 states), whereas the remaining eight states, which are in the in-component of the SCC, can reach the SCC in one step. The only difference in the transition graphs obtained from the ROA and GA methods is that the average in- and out-degrees are smaller in the GA model (where both are equal to 4) than in the ROA model (where the average in-degree is 25 and the average out-degree is 23). Note that here the whole state space is in the definite basin of attraction of the loose attractor and the eight aforementioned states are Garden-of-Eden states (not reachable from any other state). Thus this case corresponds to sustained oscillations in the sub-network, including sustained oscillations of Ca_c^{2+}, which had only a fixed point in the OFF state in the unperturbed case, and sustained oscillations of Closure, which stabilized in the ON state in the unperturbed case. For the DA

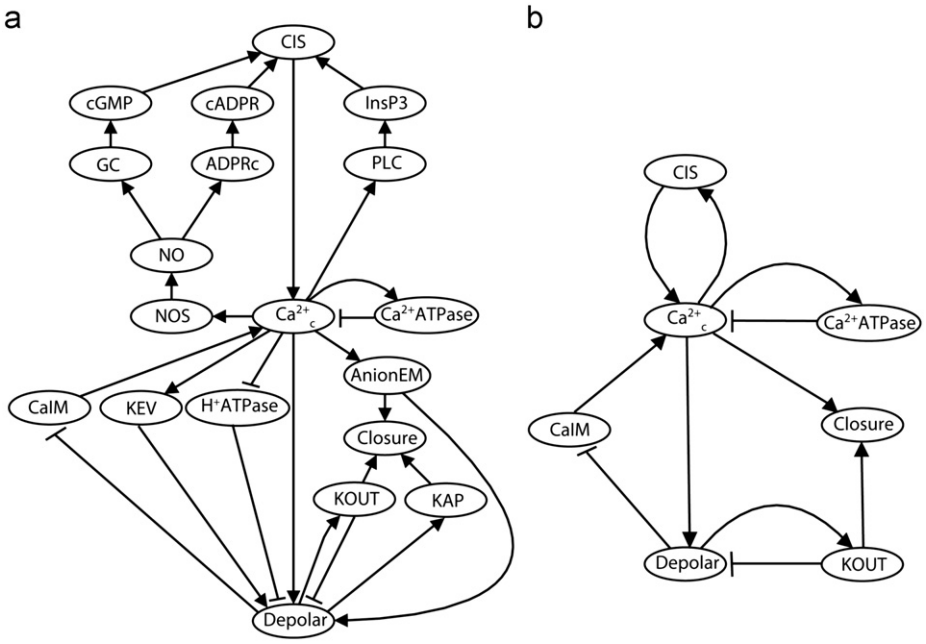

Fig. 7. The sub-network obtained by knocking out the node pH_c and its simplified version. (a) The 19-node sub-network resulting from pH_c perturbation. (b) The 7-node sub-network obtained from the network given in (a) after eliminating some of the equivalent nodes and edges.

Table 8
The Boolean functions governing the state of the nodes in the 19-node sub-network represented in Fig. 7(a).

Node	Boolean rule
NOS	NOS* = Ca_c^{2+}
NO	NO* = NOS
GC	GC* = NO
ADPRc	ADPRc* = NO
cADPR	cADPR* = ADPRc
cGMP	cGMP* = GC
PLC	PLC* = Ca_c^{2+}
InsP3	InsP3* = PLC
CIS	CIS* = (cGMP and cADPR) or InsP3
Ca^{2+}ATPase	Ca^{2+}ATPase* = Ca_c^{2+}
Ca_c^{2+}	Ca_c^{2+} * = (CaIM or CIS) and (not Ca^{2+}ATPase)
AnionEM	AnionEM* = Ca_c^{2+}
H^+ATPase	H^+ATPase* = not Ca_c^{2+}
Depolar	Depolar* = KEV or AnionEM or (not H^+ATPase) or (not KOUT) or Ca_c^{2+}
CaIM	CaIM* = not depolar
KOUT	KOUT* = depolar
KAP	KAP* = depolar
KEV	KEV* = Ca_c^{2+}
Closure	Closure* = (KOUT or KAP) and AnionEM

Table 9
The Boolean functions governing the state of the nodes in the 7-node sub-network represented in Fig. 7(b).

Node	Boolean rule
CIS	CIS* = Ca_c^{2+}
Ca^{2+}ATPase	Ca^{2+}ATPase* = Ca_c^{2+}
Ca_c^{2+}	Ca_c^{2+} * = (CaIM or CIS) and (not Ca^{2+}ATPase)
Depolar	Depolar* = (not KOUT) or Ca_c^{2+}
CaIM	CaIM* = not depolar
KOUT	KOUT* = depolar
Closure	Closure* = KOUT and Ca_c^{2+}

Table 10
The limit cycle observed in the synchronous model for the sub-network represented in Fig. 7(b).

CIS	Ca_c^{2+}	Ca^{2+}ATPase	CaIM	Closure	Depolar	KOUT
1	0	1	0	1	1	1
0	0	0	0	0	0	1
0	0	0	1	0	0	0
0	1	0	1	0	1	0
1	1	1	0	0	1	1

method, the system will have the same fixed point and it is possible that for some time units the system exhibits a limit cycle because the sub-network represented in Fig. 7(b) contains the 3-node sub-network of Fig. 3(a).

When focusing on the node Ca_c^{2+}, which is the key driver of the sub-network according to the scalar equation analysis, the difference between the 3-node sub-network and the current network is an additional negative feedback on Ca_c^{2+} mediated by the node Depolar. This negative feedback may be more effective than the negative feedback mediated by Ca^{2+}ATPase, because of the 'or' rule governing the activation of the node Depolar. We tested whether weakening the negative feedback changes the dynamics, and found, both numerically and by solving the Boolean equations, that the necessary condition for having a fixed point is a change of 'or' operation in the Boolean function of the node Depolar to 'and', and changing the inhibitory effect of Depolar on CaIM into an activation. Note that the fixed point of the whole network obtained after these rule changes is not the same as that of the wild-type network and, in particular, Closure stabilizes in the OFF state.

In summary, synchronous or DA models of the perturbed networks exhibit both limit cycles and fixed points, except for knockout of Ca_c^{2+} that results in the wild-type fixed point only and knockout of pH_c that leads only to a limit cycle. With the ROA or GA updating, the knockouts identified as leading to insensitivity by Li et al. (2006) lead to a fixed point in which half

of the nodes, including Closure, are OFF, as expected. Most of the knockouts identified as yielding reduced sensitivity will lead to a fixed point in which Closure stabilizes in the OFF state. The fixed points obtained by knocking out PA, S1P or AnionEM differ in the state of at most seven nodes. This suggests that PA and S1P knockouts that were previously reported as leading to reduced sensitivity (Li et al., 2006) can be better categorized as leading to insensitivity. An interesting exception is the perturbation of pH_c that leads to sustained oscillations for 19 nodes including Closure. The knockouts in the hypo/hyper sensitivity cases still have the wild-type fixed point with Closure stabilizing in the ON state.

4. Discussion

In this paper, we provided an investigation of the long-term dynamics of the ABA signal transduction network by applying one synchronous and three asynchronous updating methods, namely random order asynchronous, general asynchronous, and deterministic asynchronous methods. We performed a comprehensive study of all attractors of the system considering every possible initial state, changes in timing, as well as perturbations in the nodes and regulatory functions of the system. Due to the complexity of the network, we made iterative simplifications to the structure and updating rules of the original network, choosing views that support and complement each other. The topological simplifications allowed us to also determine analytically the attractors of the synchronous model by using the reduced scalar equation technique proposed by Farrow et al. (2004). Although reduced scalar equations were shown to be useful for small biological networks such as our simplified system, it should be noted that they cannot be applied to large-scale networks as the identification of the number of fixed points for monotone Boolean networks as well as determination of the existence of fixed points for general Boolean networks have been proved to be strong NP-complete problems (Zhao, 2005).

Our topological simplifications support and complement a recently proposed network reduction method by Veliz-Cuba (2009), which came to our attention after completing our analysis. This method contains two steps: 1) simplifying Boolean functions using Boolean algebra, and deleting the resulting nonfunctional edges; 2) sequentially deleting the nodes with no self loops (Veliz-Cuba, 2009). The first step is similar to the first step of our method, however we consider not only simplifications induced by redundant Boolean functions (which are a modeling artifact and may be rare) but also by stable signals in the biological system (which are system-driven and quite common). The second step is similar to our collapsing of nodes, and it is very effective when one is only interested in fixed points, however it may lead to drastic information reduction. Indeed, fixing the unregulated nodes in the ON state and applying the Veliz-Cuba method to the whole ABA network leads to a single-node network with the Boolean function $Ca_c^{2+*}=0$. As a result, the reduced network has only one fixed point, implying, based on Veliz-Cuba's results, that the original network must have a unique fixed point, which confirms our result. However, the reduced network is not informative regarding the possibility of extended attractors. Applying this reduction method to the networks obtained after pH_c knockout results in a 3-node network with the following Boolean rules:

Ca_c^{2+*} = not Depolar and not Ca_c^{2+}

Depolar* = not Depolar or Ca_c^{2+}

Closure* = Depolar and Ca_c^{2+}

It can be easily seen that this reduced network does not have any fixed points, implying that the original system affected by pH_c knockout does not have any fixed points either, which again confirms our result.

Another study on simplifying Boolean networks (Richardson, 2005) is based on removal of frozen nodes (stable variables) and network leaves (i.e. nodes with out-degree=0). A random sampling method of the initial states is used to determine a subset of the attractors, and the nodes whose state is the same in all attractors are included in a putative minimum set of frozen nodes. This method is not useful for reducing the 13-node sub-network as the minimum set of frozen nodes for this network is empty. The method may be used for reduction of the 39-node full network to the 13-node sub-network, but it would be an inefficient alternative to what we have done.

A recently introduced asynchronous Boolean model reduction method (Tournier and Chaves, 2009) consists of simplifying the model's state transition graph into a directed acyclic graph of its strongly connected components, and then identifying the subset of interactions that are operational in each strongly connected component of the state transition graph. This method is applicable to networks of eight to fifteen nodes, thus its combination with our elimination of frozen nodes may be very informative.

Markov chains have been previously employed in the study of probabilistic Boolean networks by incorporating uncertainty in the Boolean rules governing the state of the nodes (Kim et al., 2002; Shmulevich et al., 2002a; Shmulevich et al., 2002b). In this study we have provided an added insight into how Markov chain techniques can be used to analyze the dynamic behavior of systems whose uncertainty is not in the logic functions controlling the states of the nodes but in the timing of the interactions (Chaves et al., 2005; Tournier and Chaves, 2009). Particularly, we showed that the transition graph corresponding to the random order or general asynchronous models is in fact a Markov chain, thereby the absorption times to the fixed point can be obtained.

This work provides further insights into the role of the Ca_c^{2+} oscillations. We found that the Ca_c^{2+} oscillations eventually disappear in the wild-type system, unless strict constraints regarding the timing of certain processes and the initial state of the system are satisfied. For example, we found that in the deterministic asynchronous model of the 3-node reduced network, only timing values that correspond to a restricted update sequence, i.e. Ca^{2+}ATPase, Ca_c^{2+}, Ca^{2+}ATPase, Ca_c^{2+} and a few variants of it, and only two of sixteen possible initial conditions, lead to a limit cycle. Assuming that all node or node combination updates have equal probability, the estimated incidence of cycle-inducing update sequences is 64 of 2401, or 2.7%. Currently there is insufficient experimental information to gauge whether these constraints are biologically satisfied or not. However, the requirement for a longer time scale for CIS than the other two nodes is supported by the longer positive feedback loops (that involve Ca_c^{2+} and CIS) than the negative feedback loop (of Ca_c^{2+} and Ca^{2+}ATPase) in the original network (Fig. 2). Interestingly, we found that the system converges to a loose attractor when perturbing the node pH_c. In this case the Ca_c^{2+}-driven oscillations do play an observable beneficial role by leading to an at least fluctuating stomatal closure.

Our analysis refines previous results on the relative ranking of node disruptions in the ABA system. We find that from the standpoint of the long-term behavior there are only three categories of responses: knockouts leading to the wild-type fixed point (which represent 75% of all knockouts), knockouts leading to the null fixed point (22.5% of all knockouts), and a single knockout leading to sustained fluctuations.

Our study provides a roadmap to compare and verify the existence of different types of attractors resulting from Boolean

models. The important steps along the road are simplification of the network by elimination of frozen nodes and collapse of intermediary nodes, and analysis of the state transition graphs that correspond to synchronous as well as stochastic and deterministic asynchronous models. For the ABA signaling system investigated here we found both agreement (a common fixed point) and disagreement in the possibility of limit cycles among the models. We also found update-dependent diversity in the basin of attraction of the attractors, and in the case of the DA model we surprisingly found some states that are part of an attractor but not part of its basin of attraction.

The results presented in this study support the necessity of using asynchronous update in Boolean models of biological systems. The two periodic attractors whose basins of attraction dominated the synchronous model were nonexistent or had a much reduced basin in asynchronous models. This observation is consistent with previous reports (Faure et al., 2006; Mochizuki, 2005) that synchronous models possess spurious cycles. While there is increasing evidence for the necessity of relaxing the assumption of synchronicity, what kind of asynchronous implementation to use is an open question. The most definitive information, experimental data on timing and kinetics, is rarely available. It is thus very important to study what conclusions are robust to changes in the implementation of time. Our results suggest that sustained oscillations are much less prevalent than asymptotic behavior in real biological systems having a variety of time scales. This supports the prior findings that in sequential deterministic asynchronous models of networks without negative loops (self-inhibition) all dynamical cycles can be destroyed by a change in the update method (Aracena et al., 2009) and that cycles are not likely to be observed in asynchronous cellular automata models (Schonfisch and de Roos, 1999). However, we also find that focusing solely on the fixed points is not sufficient to capture all dynamical aspects of a system either, as extended attractors are possible both for deterministic and stochastic asynchronous models.

At present no asynchronous method was demonstrated to be optimal: deterministic methods require knowledge of the nodes' time units while stochastic methods have a large number of possible state transitions. In cases when no biological timing information is available, the GA method may be practically preferable over the ROA method, as it is computationally more efficient and the state transition graph of the ROA method can be obtained from the state transition graph of the GA method. For biological systems with some, but insufficient information on time scales, the middle road of imposing restrictions on the order of update (e.g. by always updating a certain node before another, see Chaves et al., 2005; Thakar et al., 2007) or on the probability of a node's update (Tournier and Chaves, 2009) may be most practical.

Acknowledgements

This work was supported by NSF Grant CCF-0643529. The authors would like to thank Prof. Mark Levi for useful discussions.

Appendix A. Deriving the reduced scalar equation for the node Ca_c^{2+} for the synchronous model of the 11-node sub-network

We note that the Boolean operators 'and', 'or', and 'not' can be expressed by the following algebraic equations:

A and $B = AB$

A or $B = A+B+AB$

not $A = 1+A$

Then the scalar equation corresponding to the node Ca_c^{2+} given in Table 3 can be written as the following:

$$\begin{aligned}Ca_c^{2+}(t+6) &= [Ca_c^{2+}(t) \text{ or } Ca_c^{2+}(t+2)] \text{ and } [\text{not } Ca_c^{2+}(t+4)]\\ &= [Ca_c^{2+}(t)+Ca_c^{2+}(t+2)+Ca_c^{2+}(t)Ca_c^{2+}(t+2)][1+Ca_c^{2+}(t+4)]\end{aligned}$$

or equivalently,

$$\begin{aligned}Ca_c^{2+}(t+6) &= Ca_c^{2+}(t)+Ca_c^{2+}(t)Ca_c^{2+}(t+4)+Ca_c^{2+}(t+2)\\ &+Ca_c^{2+}(t+2)Ca_c^{2+}(t+4)+Ca_c^{2+}(t)Ca_c^{2+}(t+2)\\ &+Ca_c^{2+}(t)Ca_c^{2+}(t+2)Ca_c^{2+}(t+4)\end{aligned} \tag{A.1}$$

Iterating the Boolean rule of Ca_c^{2+} and substituting the term $Ca_c^{2+}(t+6)$ from Eq. (A.1) we obtain

$$\begin{aligned}Ca_c^{2+}(t+8) &= Ca_c^{2+}(t+2)+Ca_c^{2+}(t+2)Ca_c^{2+}(t+6)\\ &+Ca_c^{2+}(t+4)+Ca_c^{2+}(t+4)Ca_c^{2+}(t+6)\\ &+Ca_c^{2+}(t+2)Ca_c^{2+}(t+4)\\ &+Ca_c^{2+}(t+2)Ca_c^{2+}(t+4)Ca_c^{2+}(t+6)\\ &= Ca_c^{2+}(t+2)+Ca_c^{2+}(t)Ca_c^{2+}(t+2)\\ &+Ca_c^{2+}(t)Ca_c^{2+}(t+2)Ca_c^{2+}(t+4)\\ &+[Ca_c^{2+}(t+2)]^2+[Ca_c^{2+}(t+2)]^2Ca_c^{2+}(t+4)\\ &+Ca_c^{2+}(t)[Ca_c^{2+}(t+2)]^2\\ &+Ca_c^{2+}(t)[Ca_c^{2+}(t+2)]^2Ca_c^{2+}(t+4)+Ca_c^{2+}(t+4)\\ &+Ca_c^{2+}(t)Ca_c^{2+}(t+4)+Ca_c^{2+}(t)[Ca_c^{2+}(t+4)]^2\\ &+Ca_c^{2+}(t+2)Ca_c^{2+}(t+4)+Ca_c^{2+}(t+2)[Ca_c^{2+}(t+4)]^2\\ &+Ca_c^{2+}(t)Ca_c^{2+}(t+2)Ca_c^{2+}(t+4)\\ &+Ca_c^{2+}(t)Ca_c^{2+}(t+2)\\ &\times[Ca_c^{2+}(t+4)]^2+Ca_c^{2+}(t+2)Ca_c^{2+}(t+4)\\ &+Ca_c^{2+}(t)Ca_c^{2+}(t+2)Ca_c^{2+}(t+4)\\ &+Ca_c^{2+}(t)Ca_c^{2+}(t+2)[Ca_c^{2+}(t+4)]^2\\ &+[Ca_c^{2+}(t+2)]^2Ca_c^{2+}(t+4)\\ &+[Ca_c^{2+}(t+2)]^2[Ca_c^{2+}(t+4)]^2\\ &+Ca_c^{2+}(t)[Ca_c^{2+}(t+2)]^2Ca_c^{2+}(t+4)\\ &+Ca_c^{2+}(t)[Ca_c^{2+}(t+2)]^2[Ca_c^{2+}(t+4)]^2\end{aligned}$$

Noting that in mod 2 algebra $2A=0$ and $A^2=A$, we get the following reduced scalar equation:

$$Ca_c^{2+}(t+8) = Ca_c^{2+}(t+4) \tag{A.2}$$

Appendix B. Effect of changing the Boolean rules or the topology of the 8-node sub-network represented in Fig. 4 using random order and general asynchronous methods

To probe which features of the network are responsible for the dominance of the fixed point, we considered two different changes to the sub-network given in Fig. 4:

1. In the Boolean rules of the nodes Ca_c^{2+} and CIS, we changed the 'and' operator to 'or' or vice versa.
2. We changed parallel directed edges involving any four nodes to cross edges (i.e. changed edges A→B and C→D into A→D and C→B) in such a way that the change affects the length of the positive and negative feedback loops.

While one may expect that requiring synergy between the two positive feedback loops may weaken the strongly connected component and strengthen the fixed point, our simulations with the random order asynchronous model indicate that if we change the rule of CIS from the 'or' operator to the 'and' operator, the

results do not change significantly. The size of the SCC decreases to 227 and its average in (out)-degree decreases to 24 (31). Changing the 'and' operator in the Boolean rule for Ca_c^{2+} to the 'or' operator means that the negative feedback loop loses its effectiveness. In this case we found a different fixed point in which all the nodes are in the ON state (instead of the OFF state for the original network). Interestingly, the SCC shows a similar reduction in size and connectivity as in the previous case. The results obtained from the general asynchronous model are similar to those obtained by the random order model with the significant difference in the average in and out-degrees of the SCC which are remarkably less in the GA than in the ROA model.

One of the interesting results for topological changes is that a long positive feedback loop of length six and a short one of length three leads to a larger and denser SCC, while having positive feedback loops of length two (containing the nodes CIS and Ca_c^{2+}) and seven leads to a smaller and sparser SCC. Another observation is that increasing the length of the negative feedback loop by one does not change the results but increasing it by two causes the network to have two SCCs (of sizes 87 and 84) rather than one. In this case the bigger SCC is part of the out-component of the smaller one. In the general asynchronous model these two SCCs are of the same size (88) with the first SCC being in the out-component of the other and the second SCC being in the in-component of the first one. In conclusion, regardless of the updating scheme, the SCC seems to be strongest when the size of the shorter positive feedback loop is greater than or equal to the size of the negative feedback loop. This requirement is consistent with a need to restore the state of Ca_c^{2+} to ON after it was turned OFF by the negative feedback. Nevertheless, none of the topological changes is able to strengthen the SCC to the point of becoming a loose attractor.

Appendix C. Proof of Propositions 2–5

Proposition 2. *If $t_{Ca_c^{2+}} = 2k$, where k is a positive integer number, $t_{Ca^{2+}ATPase} = 2$ and $t_{CIS} = 2t_{Ca_c^{2+}}$, then the transition graph of the 3-node sub-network has a limit cycle of length $t_{Ca_c^{2+}}$.*

Proof. As explained in the proof of Proposition 1, in order to find the cycles it is necessary to assume that the node CIS is ON initially, otherwise the system stabilizes at the null fixed point. Consider the following two cases:

Case 1: Ca_c^{2+} is OFF initially. In other words, the initial state of the system is either 100 or 101. We assume that the system is initially in the state 100. A similar argument works for the case where the initial state of the system is 101. The system stays at the state 100 until the time point $t=2k$ when Ca_c^{2+} is updated. The number of time steps the network visits state 100 before its state changes to 110 at time step $t=2k$ is $[(t_{Ca_c^{2+}}-2)/2]=k-1$. At time step $t=2k+2$, Ca^{2+}ATPase turns ON and so the state of the system changes to 111. The system's state remains unchanged until the time step $t=4k$ when Ca_c^{2+} is updated again. At this time step the state of the system changes to 101 and after that it returns to the original state. This cycle repeats itself over time. Therefore, the length of the limit cycle is $(k-1)+1+(k-1)+1=2k=t_{Ca_c^{2+}}$. A summary of this argument is given in Table C1.

Case 2: The node Ca_c^{2+} is in the ON state initially, i.e. the initial state of the system is either 110 or 111. Assume that the initial state of the system is 110. At $t=2$, the node Ca^{2+}ATPase is updated and the state of the system changes to 111. The system's state remains unchanged at all even time points, in which Ca^{2+}ATPase is updated, until the time point $t=2k$, when Ca_c^{2+} is updated, causing a change of state to 101. At time $t=2k+2$, the state of the system changes from 101 to 100 because Ca^{2+}ATPase is updated. The system's state remains unchanged until $t=4k=t_{CIS}$, when all the nodes are updated, causing a change of state to 010. Since CIS is turned OFF, Ca_c^{2+} will be turned OFF after some time and thus the network eventually converges to the null fixed point. □

Proposition 3. *If $t_{Ca^{2+}ATPase} = 2k+1$, where k is a positive integer number, $t_{Ca_c^{2+}} = 2$ and $t_{CIS} = 2t_{Ca^{2+}ATPase}$, then the transition graph of the 3-node sub-network has a limit cycle of length $t_{Ca^{2+}ATPase}+1$.*

Proof. The proof is similar to the proof of Proposition 1. In this proposition a limit cycle is reached from the initial state 101 or 111.

Proposition 4. *If $t_{Ca^{2+}ATPase} = 2k$, where k is a positive integer number, $t_{Ca_c^{2+}} = 2$ and $t_{CIS} = 2t_{Ca^{2+}ATPase}$, then the transition graph of the 3-node sub-network has a limit cycle of length $t_{Ca^{2+}ATPase}$.*

Proof. The proof is similar to the proof of Proposition 2. In this proposition the basin of attraction of the limit cycle contains the states 101 and 111.

Proposition 5. *If $t_{Ca_c^{2+}} = t_{Ca^{2+}ATPase} = 1$ and $t_{CIS}=4k$, where k is a positive integer, then the transition graph of the 3-node sub-network has a limit cycle of length four.*

Proof. As mentioned in the proof of Proposition 1, a necessary condition for the existence of the limit cycles is that the node CIS is ON initially, otherwise the system stabilizes at the null fixed point. Consider the following two cases:

Case 1: The node Ca^{2+}ATPase is in the ON state initially, i.e. the initial state of the system is either 101 or 111. Starting from either of these initial states, it is easy to check that after updating the nodes Ca_c^{2+} and Ca^{2+}ATPase four times simultaneously, the system will return to the initial state. The assumption $t_{CIS}=4k$ guarantees that the node CIS remains in the ON state at all time steps. Therefore, the length of the limit cycle of the system is four.

Case 2: The node Ca^{2+}ATPase is in the OFF state initially. In other words, the initial state of the system is either 100 or 110. No matter from which initial state the system starts, the node Ca_c^{2+} will be in the OFF state at time step $t=4k-1$ and thus CIS will turn OFF at time step $t=4k$. As a result, the system eventually reaches the null fixed point. □

Table C1
The state of the 3-node sub-network given in Fig. 3(a) in different time steps starting from initial state 100 obtained by the DA model with the time units given in Proposition 2.

Time / node	$t=0$	$t=2$	…	$t=2k-2$	$t=2k$	$t=2k+2$	…	$t=4k-2$	$t=4k$	$t=4k+2$
CIS	1	1	…	1	1	1	…	1	1	1
Ca_c^{2+}	0	0	…	0	1	1	…	1	0	0
Ca^{2+}ATPase	0	0	…	0	0	1	…	1	1	0

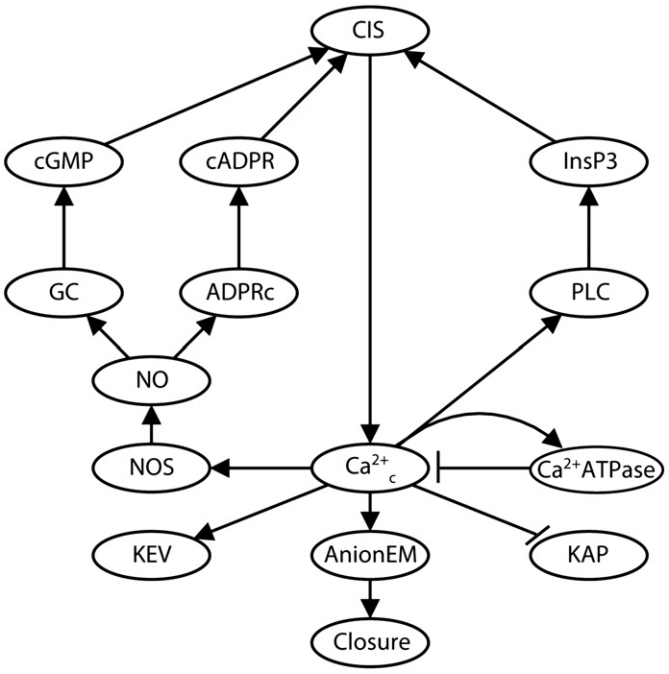

Fig. D1. The 15-node sub-network obtained from S1P or PA perturbation.

Appendix D. Results of the knockout analysis of S1P, PA, AnionEM, ABI1 or Ca_c^{2+}

After disrupting S1P or PA, most of the nodes stabilize in the ON or OFF state, leaving 15 nodes for further analysis. These nodes include the 13 nodes mentioned in Table 1 and two additional nodes, namely AnionEM and Closure. As represented in Fig. D1, the state of both AnionEM and Closure is driven by Ca_c^{2+} with some time delay. With synchronous updating, this sub-network will converge to a fixed point or one of the two limit cycles of length four as in the wild type, with the important difference that both Closure and AnionEM are OFF in the fixed point and are oscillating in the limit cycles, while in the wild type they stabilized in the ON state. For the ROA and GA methods, based on our results presented before, the network possesses only the fixed point of the synchronous update. For the DA method, the system will have the same fixed point and it is possible that for some time units the system exhibits a limit cycle because the sub-network represented in Fig. D1 contains the 3-node sub-network of Fig. 3(a).

When AnionEM is knocked out, 26 nodes stabilize within eight time steps for the synchronous method and within eight rounds of update for the ROA method and in particular Closure stabilizes in the OFF state after one time step (round of update). The other 13 nodes having fluctuations are the same as the 13-node sub-network given in Fig. 2, and will eventually converge to the null fixed point or one of the two limit cycles mentioned in Table 2 for the synchronous method. For the ROA and GA methods the sub-network only possesses the null fixed point, whereas for the DA model the sub-network has the null fixed point and may have limit cycles for certain time units.

In the case of disrupting ABI1 the network will eventually converge to the corresponding attractor(s) of the wild-type network. The node Closure stabilizes in the ON state within five time steps of synchronous update or five rounds of update in the ROA method. The reason for this earlier stabilization is that the system does not need to wait for ABI1, a node with a negative effect on closure, to turn OFF. Finally, with setting Ca_c^{2+} to the OFF state, regardless of the updating scheme, all nodes of the network stabilize and the system reaches the fixed point of the wild-type network. In particular, Closure stabilizes in the ON state within eight rounds of update.

References

Albert, I., Thakar, J., Li, S., Zhang, R., Albert, R., 2008. Boolean network simulations for life scientists. Source Code Biol. Med. 3, 16.

Allen, G.J., Chu, S.P., Harrington, C.L., Schumacher, K., Hoffmann, T., Tang, Y.Y., Grill, E., Schroeder, J.I., 2001. A defined range of guard cell calcium oscillation parameters encodes stomatal movements. Nature 411, 1053–1057.

Aracena, J., Goles, E., Moreira, A., Salinas, L., 2009. On the robustness of update schedules in Boolean networks. Biosystems 97, 1–8.

Berridge, M.J., Lipp, P., Bootman, M.D., 2000. The versatility and universality of calcium signalling. Nat. Rev. Mol. Cell Biol. 1, 11–21.

Chaves, M., Albert, R., Sontag, E.D., 2005. Robustness and fragility of Boolean models for genetic regulatory networks. J. Theor. Biol. 235, 431–449.

Chaves, M., Sontag, E.D., Albert, R., 2006. Methods of robustness analysis for Boolean models of gene control networks. Syst. Biol. (Stevenage) 153, 154–167.

Chen, K.C., Csikasz-Nagy, A., Gyorffy, B., Val, J., Novak, B., Tyson, J.J., 2000. Kinetic analysis of a molecular model of the budding yeast cell cycle. Mol. Biol. Cell 11, 369–391.

Cinquin, O., Demongeot, J., 2002. Positive and negative feedback: striking a balance between necessary antagonists. J. Theor. Biol. 216, 229–241.

Cuthbertson, K.S., Cobbold, P.H., 1985. Phorbol ester and sperm activate mouse oocytes by inducing sustained oscillations in cell Ca2. Nature 316, 541–542.

Dubrova, E., Teslenko, M., 2010. A SAT-based algorithm for computing attractors in synchronous Boolean networks. IEEE/ACM Trans. Comput. Biol. Bioinform, PrePrint.

Farrow, C., Heidel, J., Maloney, J., Rogers, J., 2004. Scalar equations for synchronous Boolean networks with biological applications. IEEE Trans. Neural Network 15, 348–354.

Faure, A., Naldi, A., Chaouiya, C., Thieffry, D., 2006. Dynamical analysis of a generic Boolean model for the control of the mammalian cell cycle. Bioinformatics 22, e124–e131.

Garg, A., Di Cara, A., Xenarios, I., Mendoza, L., De Micheli, G., 2008. Synchronous versus asynchronous modeling of gene regulatory networks. Bioinformatics 24, 1917–1925.

Giot, L., Bader, J.S., Brouwer, C., Chaudhuri, A., Kuang, B., Li, Y., Hao, Y.L., Ooi, C.E., Godwin, B., Vitols, E., Vijayadamodar, G., Pochart, P., Machineni, H., Welsh, M., Kong, Y., Zerhusen, B., Malcolm, R., Varrone, Z., Collis, A., Minto, M., Burgess, S., McDaniel, L., Stimpson, E., Spriggs, F., Williams, J., Neurath, K., Ioime, N., Agee, M., Voss, E., Furtak, K., Renzulli, R., Aanensen, N., Carrolla, S., Bickelhaupt, E., Lazovatsky, Y., DaSilva, A., Zhong, J., Stanyon, C.A., Finley Jr., R.L., White, K.P., Braverman, M., Jarvie, T., Gold, S., Leach, M., Knight, J., Shimkets, R.A., McKenna, M.P., Chant, J., Rothberg, J.M., 2003. A protein interaction map of Drosophila melanogaster. Science 302, 1727–1736.

Gouze, J.L., 1998. Positive and negative circuits in dynamical systems. J. Biol. Systems 6, 11–15.

Harvey, I., Bossomaier, T., 1997. Time out of joint: attractors in asynchronous random Boolean networks. In: Husbands, P., Harvey, I. (Eds.), Proceedings of the Fourth European Conference on Artificial Life, Cambridge, UK, pp. 67–75.

Heidel, J., Maloney, J., Ch, F., J, R., 2003. Finding cycles in synchronous Boolean networks with applications to biochemical systems. Int. J. Bifurcat. Chaos 13, 535–552.

Irons, D.J., 2009. Logical analysis of the budding yeast cell cycle. J. Theor. Biol. 257, 543–559.

Jones, K.T., 1998. Ca^{2+} oscillations in the activation of the egg and development of the embryo in mammals. Int. J. Dev. Biol. 42, 1–10.

Kauffman, S.A., 1969. Metabolic stability and epigenesis in randomly constructed genetic nets. J. Theor. Biol. 22, 437–467.

Kauffman, S.A., 1993. Origins of Order: Self-Organization and Selection in Evolution. Oxford University Press, New York.

Kim, S., Li, H., Dougherty, E.R., Cao, N., Chen, Y., Bittner, M., Suh, E.B., 2002. Can Markov chain models mimic biological regulation? J. Biol. Syst. 10 337–357.

Klemm, K., Bornholdt, S., 2005. Stable and unstable attractors in Boolean networks. Phys. Rev. E Stat. Nonlinear Soft Matter Phys. 72, 055101.

Lee, T.I., Rinaldi, N.J., Robert, F., Odom, D.T., Bar-Joseph, Z., Gerber, G.K., Hannett, N.M., Harbison, C.T., Thompson, C.M., Simon, I., Zeitlinger, J., Jennings, E.G., Murray, H.L., Gordon, D.B., Ren, B., Wyrick, J.J., Tagne, J.B., Volkert, T.L., Fraenkel, E., Gifford, D.K., Young, R.A., 2002. Transcriptional regulatory networks in Saccharomyces cerevisiae. Science 298, 799–804.

Li, S., Assmann, S.M., Albert, R., 2006. Predicting essential components of signal transduction networks: a dynamic model of guard cell abscisic acid signaling. PLoS Biol. 4, e312.

Li, S., Armstrong, C.M., Bertin, N., Ge, H., Milstein, S., Boxem, M., Vidalain, P.O., Han, J.D., Chesneau, A., Hao, T., Goldberg, D.S., Li, N., Martinez, M., Rual, J.F., Lamesch, P., Xu, L., Tewari, M., Wong, S.L., Zhang, L.V., Berriz, G.F., Jacotot, L., Vaglio, P., Reboul, J., Hirozane-Kishikawa, T., Li, Q., Gabel, H.W., Elewa, A., Baumgartner, B., Rose, D.J., Yu, H., Bosak, S., Sequerra, R., Fraser, A., Mango, S.E., Saxton, W.M., Strome, S., Van Den Heuvel, S., Piano, F., Vandenhaute, J., Sardet, C., Gerstein, M., Doucette-Stamm, L., Gunsalus, K.C., Harper, J.W.,

Cusick, T.P., Roth, F.P., Hill, D.E., Vidal, M., 2004. A map of the interactome network of the metazoan C. elegans. Science 303, 540–543.
Matache, M.T., Heidel, J., 2005. Asynchronous random Boolean network model based on elementary cellular automata rule 126. Phys. Rev. E Stat. Nonlinear Soft Matter Phys. 71, 026232.
McAinsh, M.R., Webb, A., Taylor, J.E., Hetherington, A.M., 1995. Stimulus-induced oscillations in guard cell cytosolic free calcium. Plant Cell 7, 1207–1219.
Mendoza, L., Alvarez-Buylla, E.R., 2000. Genetic regulation of root hair development in Arabidopsis thaliana: a network model. J. Theor. Biol. 204, 311–326.
Mochizuki, A., 2005. An analytical study of the number of steady states in gene regulatory networks. J. Theor. Biol. 236, 291–310.
Morita, K., Koketsu, K., Kuba, K., 1980. Oscillation of [Ca^{2+}]i-linked K+ conductance in bullfrog sympathetic ganglion cell is sensitive to intracellular anions. Nature 283, 204–205.
Mortveit, H.S., Reidys, C.M., 2007. An Introduction to Sequential Dynamical Systems. Springer, New York.
Papin, J.A., Hunter, T., Palsson, B.O., Subramaniam, S., 2005. Reconstruction of cellular signalling networks and analysis of their properties. Nat. Rev. Mol. Cell Biol. 6, 99–111.
Reichard, A., Comet, J.-P., 2007. Necessary conditions for multistationarity in discrete dynamical systems. Discrete Appl. Math. 155, 2403–2413.
Remy, E., Ruet, P., 2008. From minimal signed circuits to the dynamics of Boolean regulatory networks. Bioinformatics 24, i220–i226.
Remy, E., Ruet, P., Thieffry, D., 2008. Graphic requirements for multistability and attractive cycles in a Boolean dynamical framework. Adv. Appl. Math. 41, 335–350.
Richardson, K.A., 2005. Simplifying Boolean networks. Adv. Complex Systems 8, 365–381.
Schonfisch, B., de Roos, A., 1999. Synchronous and asynchronous updating in cellular automata. BioSystems 51, 123–143.
Schroeder, J.I., Allen, G.J., Hugouvieux, V., Kwak, J.M., Waner, D., 2001. Guard cell signal transduction. Annu. Rev. Plant Physiol. Plant Mol. Biol. 52, 627–658.
Shmulevich, I., Dougherty, E.R., Zhang, W., 2002a. From Boolean to probabilistic Boolean networks as models of genetic regulatory networks. Proc. IEEE 90, 1778–1792.
Shmulevich, I., Dougherty, E.R., Kim, S., Zhang, W., 2002b. Probabilistic Boolean Networks: a rule-based uncertainty model for gene regulatory networks. Bioinformatics 18, 261–274.
Siebert, H., 2009. Deriving behavior of Boolean bioregulatory networks from subnetwork dynamics. Math. Comput. Sci. 2, 421–442.
Song, M., Ouyang, Z., Liu, Z.L., 2009. Discrete dynamical system modelling for gene regulatory networks of 5-hydroxymethylfurfural tolerance for ethanologenic yeast. IET Syst. Biol. 3, 203–218.
Sontag, E., Veliz-Cuba, A., Laubenbacher, R., Jarrah, A.S., 2008. The effect of negative feedback loops on the dynamics of Boolean networks. Biophys. J. 95, 518–526.
Thakar, J., Pilione, M., Kirimanjeswara, G., Harvill, E.T., Albert, R., 2007. Modeling systems-level regulation of host immune responses. PLoS Comput. Biol. 3, e109.
Thomas, R., 1973. Boolean formalization of genetic control circuits. J. Theor. Biol. 42, 563–585.
Thomas, R., 1981. On the relation between the logical structure of systems and their ability to generate multiple steady states and sustained oscillations. In: Numerical Methods in the Study of Critical Phenomena, vol. 9. Springer Verlag, Berlin, pp. 180–193.
Thomas, R., D'Ari, R., 1990. Biological Feedback. CRC Press, Boca Raton.
Tournier, L., Chaves, M., 2009. Uncovering operational interactions in genetic networks using asynchronous Boolean dynamics. J. Theor. Biol. 260, 196–209.
Tuchwell, H., 1988. Elementary Applications of Probability Theory. Chapman & Hall.
Veliz-Cuba, A., 2009. Reduction of Boolean networks. arXiv:0907.0285v1.
von Dassow, G., Meir, E., Munro, E.M., Odell, G.M., 2000. The segment polarity network is a robust developmental module. Nature 406, 188–192.
Willadsen, K., Wiles, J., 2007. Robustness and state-space structure of Boolean gene regulatory models. J. Theor. Biol. 249, 749–765.
Wuensche, A., 2002. Basins of attraction in network dynamics: a conceptual framework for biomolecular networks. In: Schlosser, G., Wagner, G.P. (Eds.), Modularity in Development and Evolution. Chicago University Press, pp. 288–311.
Zhang, R., Shah, M.V., Yang, J., Nyland, S.B., Liu, X., Yun, J.K., Albert, R., Loughran Jr., T.P., 2008. Network model of survival signaling in large granular lymphocyte leukemia. Proc. Natl. Acad. Sci. USA 105, 16308–16313.
Zhao, Q., 2005. A remark on "Scalar equations for synchronous Boolean networks with biological applications" by C. Farrow, J. Heidel, J. Maloney, and J. Rogers. IEEE Trans. Neural Network 16, 1715–1716.